

Short-term episodes of carbonate productivity in a Cambrian uplifted rift shoulder of the Coastal Meseta, Morocco

J. Javier Álvaro^{a,b,*}, Hassan Ezzouhairy^c, N. Ait Ayad^c, A. Charif^c,
Leonid Popov^d, M. Luisa Ribeiro^e

^a Departamento Ciencias de la Tierra, Universidad de Zaragoza, 50009 Zaragoza, Spain

^b UMR 8157, Université de Lille I, 59655 Villeneuve d'Ascq, France

^c Département de Géologie, Université Chouaib Doukkali, 24000 El Jadida, Morocco

^d National Museum of Wales, Cathays Park, Cardiff CF10 3NP, UK

^e INETI - Área de Geociências, Estrada da Portela, Zambujal, 2721-866 Alfragide, Portugal

Received 11 February 2008; received in revised form 8 April 2008; accepted 12 April 2008

Available online 22 April 2008

Abstract

This paper presents an analysis of the spatiotemporal distribution and composition of a volcanosedimentary complex, which has recorded a significant episode of carbonate productivity embedded in a thick and monotonous, turbiditic-dominated rift succession. The studied nucleation of a microbial–skeletal carbonate factory is middle Cambrian in age and situated at Sidi-Saïd-Mâachou, an uplifted rift shoulder of the Moroccan Coastal Meseta located at the junction of several graben segments, where an alkaline basaltic magma was extruded along fissures or intruded as sills and dikes.

The geometry and facies of the skeletal calcarenite sheets, composed of hiatal shelled accumulations separated by microbial mats, is comparable to those of the Brèche à *Micmacca* recorded across the lower-middle Cambrian transition in the Anti-Atlas and High Atlas. The patchy and diachronous distribution of these ‘anomalous’ carbonate factories, spatially and temporally associated with volcanic episodes, marks the northward migration of active rifting structures throughout the Moroccan margin of West Gondwana.

© 2008 International Association for Gondwana Research. Published by Elsevier B.V. All rights reserved.

Keywords: Carbonate productivity; Alkaline basalt; Rifting; Cambrian; West Gondwana

1. Introduction

Synsedimentary tectonic activity and volcanism are two major factors that control the location, size, and shape of carbonate substrates in rift basins. Extensive segmentation of their platforms into faulted blocks can be responsible for the nucleation of carbonate factories in areas shielded from effusive volcaniclastic input (e.g., Wilson, 2000; Wilson and Lockier,

2002; Fernández-Mendiola and García-Mondéjar, 2003; Álvaro and Clausen, 2007). The geochemical affinity of volcanic products is a primary factor that controls the explosive character of effusions and the quantity of volcaniclastic ejecta (Wallace and Anderson, 2000): the onset of explosive volcaniclastic ejecta is characteristic of felsic eruptions, whereas the effusion of basic lava flows under calm conditions does not necessarily yield significant quantities of volcaniclastic material. As a result, the setting of basic volcanic vents can play an important role in the nucleation of anomalous carbonate factories, linked to the release of hydrothermal fluids and the mineralogical changes of basaltic lavas (triggering microbial ‘blooms’) and/or local modifications of nutrients, substrate, and depth conditions (Van Dover, 2000).

The Ediacaran-middle Cambrian rift basin located in the Moroccan margin of West Gondwana (see recent syntheses of

* Corresponding author. Departamento Ciencias de la Tierra, Universidad de Zaragoza, 50009 Zaragoza, Spain. Tel.: +34 976761000.

E-mail addresses: Jose-Javier.Alvaro@univ-lille1.fr (J.J. Álvaro), ezzouhairy_hassan@yahoo.fr (H. Ezzouhairy), aitayad@hotmail.com (N.A. Ayad), abdelcharif@hotmail.com (A. Charif), leonid.popov@museumwales.ac.uk (L. Popov), mluisa.ribeiro@ineti.pt (M.L. Ribeiro).

the latter in Goscombe and Gray, 2008; Vaughan and Pankhurst, 2008) offers an excellent opportunity to assess the coeval influence of tectonic and volcanic activity on the spotty appearance of shelly and microbial carbonate factories punctuating homogeneous shale successions, several kilometres thick. The phase of intra-continental extension that took place in this Gondwanan margin, post-dating the end of the Pan-African orogeny (El Baghdadi et al., 2001, 2003; Martin et al., 2003; Meert and Lieberman, 2008; Stern, 2008), led to the development of a multi-segmented rift, which propagated northward over a distance of *ca.* 1000 km, and finally aborted during late middle Cambrian times (Piqué et al., 1995; Soulaimani et al., 2003). The magmatism associated with this intra-plate extension shows tholeiitic and alkaline affinities, and a distinct diachronous character: it started earlier (latest Neoproterozoic) in the Anti-Atlas (Gasquet et al., 2005; Álvaro et al., 2006, 2008; Ezzouhairi et al., 2008), reached the western High Atlas after the earliest Cambrian (Badra et al., 1992; Ait Ayad et al., 1998), and propagated even later in the Coastal Meseta (Ouali et al., 2000, 2003).

This paper is focused on one of the youngest Cambrian volcanic events recorded in the Coastal Meseta of Morocco: the so-called Sidi-Saïd-Maâchou volcano (Gigout, 1956). We undertook a study of the volcanic units and the encasing sediments of its volcanosedimentary complex to constrain the carbonate productivity, sedimentary evolution, and geometry recorded in an anomalous uplifted area located at a junction of several graben segments (Bernardin et al., 1988; Roussel and Bernardin, 1991).

2. Geological setting and stratigraphy

In the Coastal Meseta of Morocco (Fig. 1A), a thick lower Palaeozoic succession is known from exposure along the Oum-Rbia oued and its SE prolongation, the Rehamna massif, and from core drilling under the Mesozoic–Cenozoic cover in the Doukkala Plateau (or Essaouira Basin; Fig. 1B). Cambrian strata have been subdivided there into three units (Gigout, 1951, 1956; Destombes and Jeannette, 1966; Michard, 1976; Corsini, 1988; Fig. 2A), in ascending order: (i) the so-called ‘Schistes à Paradoxides’, middle Cambrian in age, and composed of more than 1000 m of homogeneous green shales and greywackes, locally interrupted by volcanosedimentary units containing carbonate strata; (ii) the El Hank Formation, *ca.* 30 m thick, which consists of sandstones, quartzites and subsidiary shales, considered as uppermost middle Cambrian; and (iii) a lithostratigraphically informal shale-dominated unit, more than 200 m thick, which has yielded Furongian brachiopods at Sidi-Saïd-Maâchou (Corsini, 1988) and Imfout (El Attari and Hoepffner, 1997). The basement of the ‘Schistes à Paradoxides’ is unknown, and the thickness of the entire Cambrian shows important lateral modifications: it ranges from *ca.* 2000 m at Sidi-Saïd-Maâchou to *ca.* 4000 m at Imfout, and from 3000 to 7000 m in subsurface reflecting the arrangement of the Cambrian rift basin in palaeohigh and graben segments (Bernardin et al., 1988; Fig. 1B).

Biostratigraphically significant fossils are scattered in the ‘Schistes à Paradoxides’ of the Rehamna massif and its northern prolongation along the Oum-Rbia oued. Gigout (1951)

reported the finding of trilobites in four disconnected outcrops: in the vicinity of Casablanca, Imfout, Mechra-ben-Abiou, and Sidi-Saïd-Maâchou (Fig. 1B). The trilobite assemblage consists of *Badulesia tenera* (Hartt in Dawson, 1868), *Conocoryphe brevifrons* Thoral, 1946, *Kingaspis maroccana* (Gigout, 1951), and other paradoxidid and conocoryphid undeterminable debris. The two first species allow correlation of these strata with the early Caesaraugustan–middle Languedocian (middle Cambrian) of southwestern Europe (Álvaro and Vizcaíno, 1998). This middle Cambrian conocoryphid–paradoxidid–solenopleurid assemblage represents the conocoryphid biofacies that developed in deep, turbid waters throughout West Gondwana (Álvaro and Vizcaíno, 2003).

In the northeastern part of the Hercynian Moroccan Meseta, a volcanosedimentary unit, named Oued-Rhebar Volcanic Complex by El Hadi et al. (2006), occurs interbedded in the ‘Schistes à Paradoxides’. The authors related the complex to a SW–NE-trending palaeogeographic horst in a subsiding rift setting. The structure is considered to be the northern prolongation of the middle Cambrian western Meseta graben (Bernardin et al., 1988; El Hadi et al., 2006). The volcanic rocks include andesites, trachyandesites, cinerites, pyroclastic tuffs, breccias, dikes, sills, and pillow and flow lavas, and show a calc-alkaline geochemical affinity (Destombes and Jeannette, 1966; Piqué, 1979; El Hadi et al., 2006).

A middle Cambrian volcanism is also known at Sidi-Saïd-Maâchou and Haute-Moulouya, where it shows a within-plate alkaline nature (Ouali et al., 2000, 2001), tholeiitic at Bou-Acila (Khénifra; Ouali et al., 2003) in the southeastern part of central Morocco (Ouali et al., 2001, 2003), and calc-alkaline at Rhebar oued (El Hadi et al., 2006). In the latter, the Hercynian deformation is related to the SW–NE-trending El-Haj-Thami shear zone (Cailleux et al., 1989; Laamrani El Idrissi, 1995), a tectonic line inherited from the middle Cambrian rifting (Piqué, 1979, 2003; Bernardin et al., 1988; Piqué and Michard, 1989; Piqué et al., 1995).

3. Mineralogy and geochemistry of volcanic rocks

The Cambrian exposures of Sidi-Saïd-Maâchou are longitudinally cut by the Oum-Rbia oued. They are unconformably capped by Permo-Trias and Pliocene strata and can be identified both in the Sidi-Moul-Nker and Aïn-Bel-Gorchi jbel (Gigout, 1956; Fig. 1C). The area is well exposed and relatively undeformed: the strata are close to the horizontal or display gently monoclinal folds (crest lines trend approximately NNE–SSW), with a broad NNE–SSW-trending direction.

The stratigraphic log shown in Fig. 2 was measured in the Sidi-Moul-Nker jbel dipping *ca.* 10° to the ESE. There, the ‘Schistes à Paradoxides’ unit includes a volcanosedimentary complex, formed by a broad lenticular sedimentary body, up to 10 km across and *ca.* 16 m thick, embedded in a thick and homogeneous shale/greywacke succession. The complex consists of lava flows, dike intrusions, conglomeratic and breccia lenses, and limestone beds embedded in a green and purple, shale-dominated succession that displays interbedded tuffs and tuffites upsection (Gigout, 1951, 1956). Gigout (1956) mapped

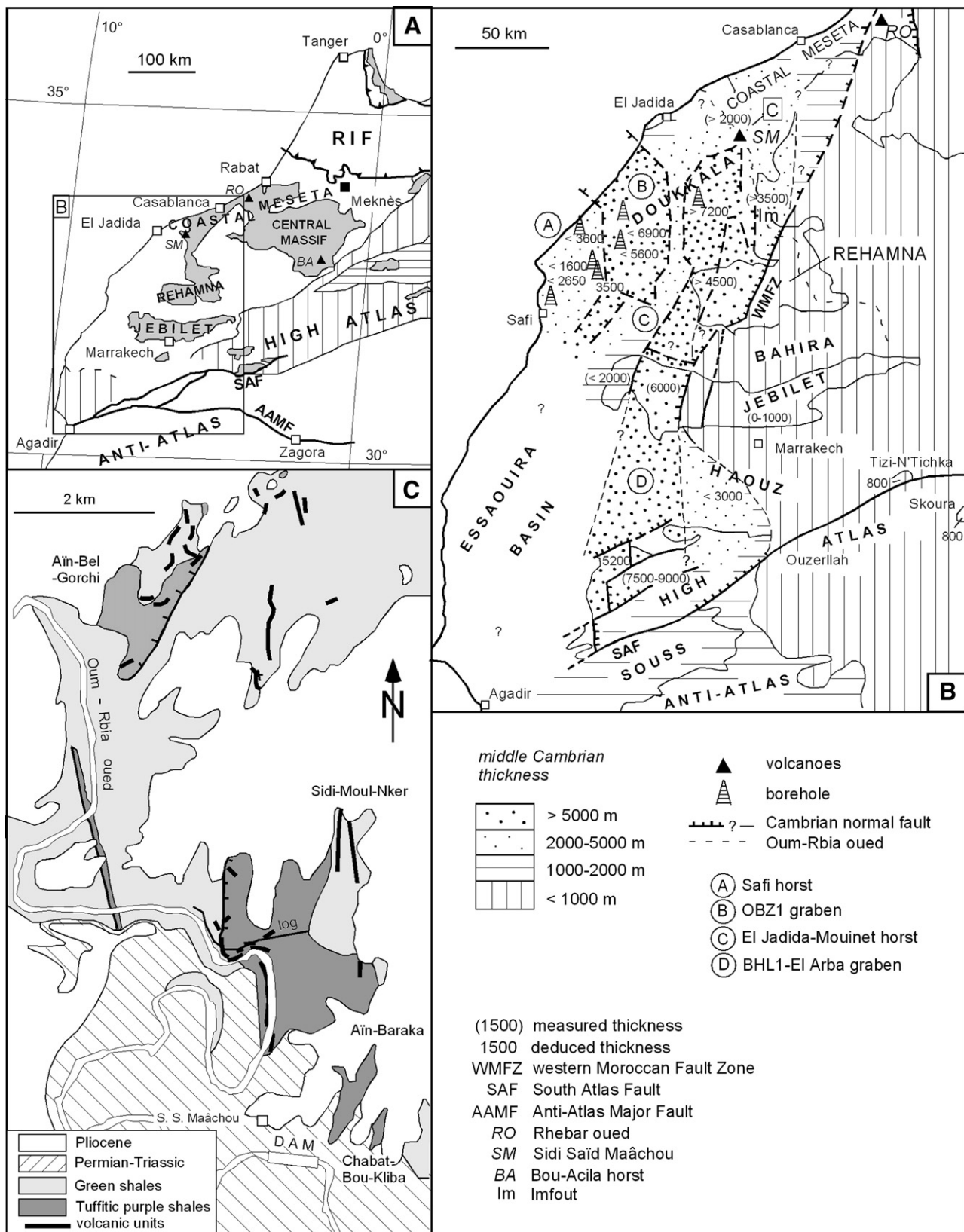


Fig. 1. A. Pre-Hercynian outcrops of the northwestern edge of Africa showing their major tectonostratigraphic units (modified from Michard, 1976). B. Geological sketch of the Cambrian thickness modifications in the Coastal Meseta, Central Massif, Rehamna and Jebilet Ranges, Morocco (modified from Bernardin et al., 1988). C. Cambrian stratigraphic units cropping out along the Oum-Rbia oued (modified from Gigout, 1951, 1956).

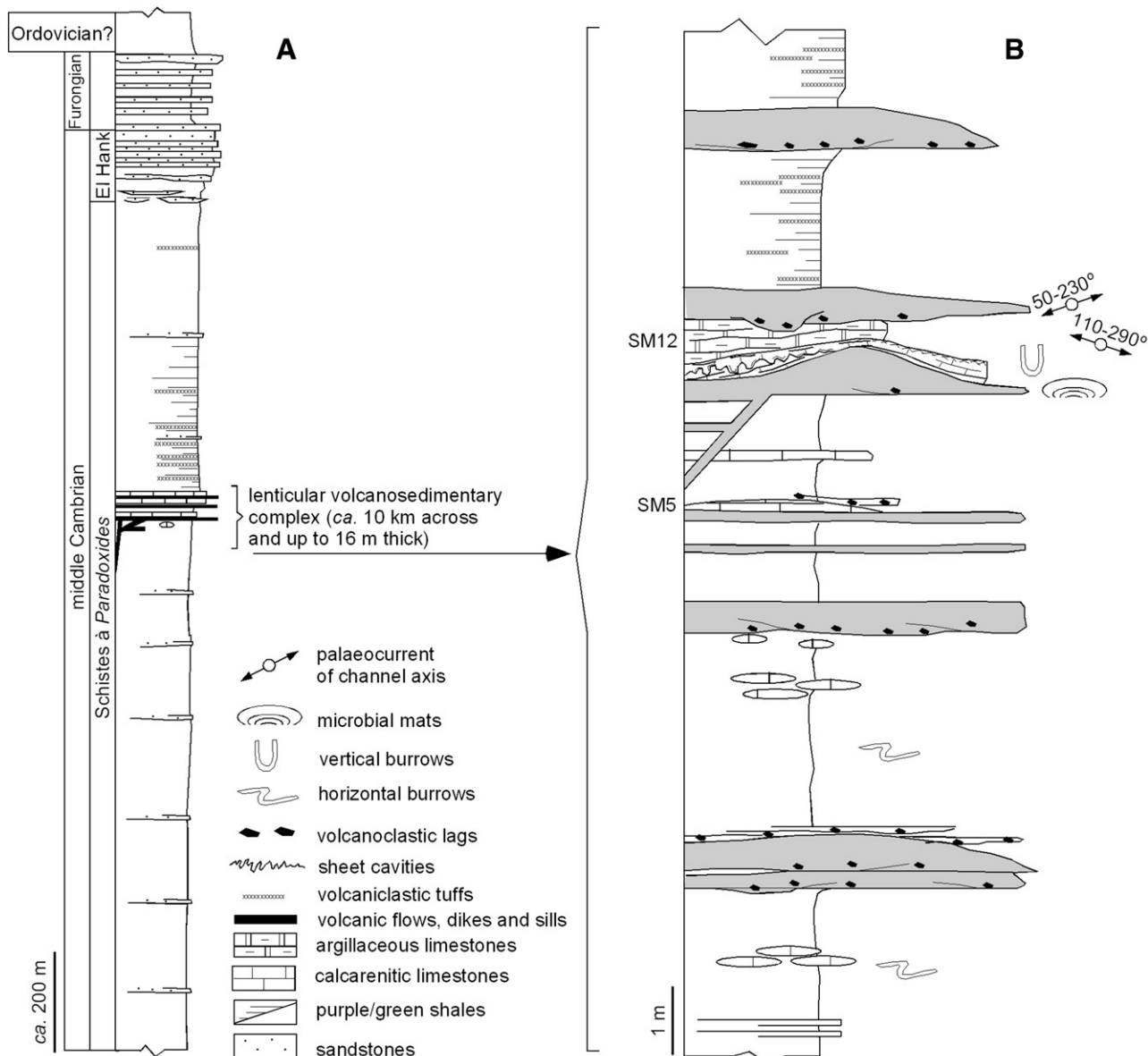


Fig. 2. A. Cambrian stratigraphic units of the Coastal Meseta. B. Stratigraphic log of the middle Cambrian volcanosedimentary complex measured at the Sidi-Moulker jbel, in the vicinity of Sidi-Saïd-Mâachou.

the area in detail and pointed out the absence of lava flows, dikes and sills in surrounding areas (e.g., in Aïn-Baraka and Chabat-Bou-Kliba, located 2 km and 5 km to the SE, respectively; Fig. 1C). Although Gigout (1956) named this volcanosedimentary complex the ‘Sidi-Saïd-Mâachou volcano’, it is herewith described as a ‘flood basalt field’ (*sensu* Kilburn, 2000), which consists of non-voluminous spreads of lava flows, erupted from scattered monogenetic fissures.

The volcanogenic units of Sidi-Saïd-Mâachou can be subdivided into: (i) *in situ* (lava flows and intrusions) and (ii) reworked (breccias, conglomerates, and tuffs) types, which will be described below separately. Chimneys infilled with breccia are absent. Coherent lava flows are up to 1 m thick; they are locally underlain by polymictic volcanic conglomerate and breccia lags, up to 10 cm thick, and occur laterally surrounded by volcaniclastic breccias and conglomerates. The thicker lava

units are tabular and extend for >50 m along strike areas, whereas the volcaniclastic units (up to 40 cm thick) are irregular in shape and cannot be followed beyond 20 m. Lava flows are variably vesicular (0–40% in volume), with higher densities concentrated on their tops displaying bedding-parallel vesicle layers. The top of the volcanic lava flows contains subvertical fissures, several centimetres wide, bearing irregular pockets of autoclastic breccia. Single eruptions seem to be related to lineated sheet-like flows near the volcanic vents, gradually degrading downstream to lobate flows, as local effusion rate declines and the flow spread outward (Gregg and Fink, 1995). Pillow lavas at flow margins are absent, probably constrained by the effusion and cooling rates, and the lack of significant slopes. The surface distribution and volume of lava flows are more important to the South than to the North of the study area (Fig. 1C), which suggest a southward slight palaeoslope.

Subvolcanic intrusive rocks formed vertical dikes, from which the magma fed lava flows and synsedimentary sills, both up to 0.8 m wide. The dike network crosscutting bedded shales and limestones is primarily oriented ENE–WSW, with subsidiary NNE–SSW and E–W orientations.

All the volcanic rocks that form the Sidi-Saïd-Mâachou flood basalt field display micro-porphyritic textures, changing into doleritic textures in the dykes that fed the lava flows. The mineralogical association of these rocks is dominated by phenocrysts of plagioclase (*ca.* An₆₀), *ca.* 10 mm in size, and ferromagnesian minerals. Although the outline and cleavage of the latter mimic those of olivine and pyroxene, they are completely replaced by calcite, chlorite, and leucoxene. The fine-grained matrix, reaching *ca.* 55% in rock volume, is essentially composed of plagioclase microliths (compositionally similar to the phenocrysts) and several oxides (chromite, ilmenite, and rutile) and sulfides (idiomorphic pyrite, sphalerite, and galena).

The geochemical analysis of ten representative samples selected in the Sidi-Saïd-Mâachou flood basalt field (see Table 1)

shows a high LOI (loss on ignition) ranging from 7.5 to 11.5%. This is likely associated with water–rock interaction processes after lava production under very low-grade metamorphic conditions. The geochemical analyses displayed in the following figures and text have been recalculated to 100% on a water-free basis, following recommendations of the IUGS (Le Maitre et al., 1989). The basaltic composition of these rocks shows a large variation in SiO₂ (45% < SiO₂ < 50%) with low K₂O contents (< 1.78%), high TiO₂ (> 2%), and Ni and Cr values ranging from 50 to 240 ppm and 130 to 340 ppm, respectively. The Mg# index, ≤ 0.38, indicates that these basalts are differentiated and do not represent primitive liquids. The Y/Nb ratio (< 1), and the SiO₂ versus TAS and FeO*/MgO versus TiO₂ diagrams displayed by the basaltic dykes, sills, and flows (Fig. 3A–B) indicate these rocks belong to the alkaline field of an intra-plate domain. The spider diagrams (Fig. 3C) display LILE, Zr, and LREE enriched patterns (La/Lu = 95). The unusual positive Zr anomaly could be explained by crustal contamination. The projection on the Crowley et al.'s (2000) diagram (Fig. 3D)

Table 1
Major (%) and trace (ppm) element analysis of middle Cambrian basaltic rocks from Sidi-Saïd-Mâachou; the geochemical data were analysed at the INETI laboratory, Porto; LOI: loss on ignition; Fe₂O₃: total iron

Sample	BMF	BM6	BM9	BM7	BM3	BM2	BM1	BM8	BM5	BM4
SiO ₂	41.01	41.02	41.08	43.20	43.26	43.76	43.89	44.24	45.72	44.82
Al ₂ O ₃	14.77	14.67	13.97	14.54	15.03	16.29	15.23	15.32	14.62	14.95
Fe ₂ O ₃ t	13.14	11.43	13.65	12.90	11.21	11.54	10.92	12.62	11.66	11.26
MnO	0.32	0.22	0.39	0.18	0.20	0.17	0.20	0.16	0.17	0.17
MgO	5.02	6.22	4.66	9.14	6.15	6.09	6.34	7.95	6.91	6.09
CaO	8.16	10.04	8.66	6.23	8.95	7.65	8.39	6.92	5.90	8.17
Na ₂ O	1.72	2.32	1.58	1.73	2.80	2.97	2.78	1.85	2.67	2.72
K ₂ O	1.49	0.73	1.57	1.32	0.67	0.70	0.67	0.78	1.07	0.81
TiO ₂	2.19	2.25	2.25	1.95	2.43	2.60	2.46	2.08	2.37	2.42
P ₂ O ₅	0.44	0.42	0.46	0.31	0.46	0.52	0.47	0.33	0.45	0.49
LOI	11.41	10.44	11.51	8.08	8.67	7.48	8.45	7.57	8.35	7.92
Total	99.67	99.76	99.78	99.58	99.83	99.77	99.8	99.82	99.89	99.82
Ni		152		236	66	53	62	152	84	78
Cr		253		339	152	130	147	279	166	162
Co		55		59	34	41	39	54	41	41
Zn		95		228	127	102	110	161	125	104
Rb	41	11	42	19	5	7	6	12	20	7
Sr	267	466	223	336	451	605	474	384	224	573
Y	17	16	17	15	18	20	18	15	18	18
Zr	174	183	172	129	194	234	199	135	181	212
Nb	30	27	31	24	30	35	30	25	30	32
Ba	171	169	159	273	251	346	264	326	169	338
Ta	1.8	1.62	2	1.4	1.8	2.1	1.8	1.5	1.8	1.9
La	23.7	20.4		15.7		25.3				
Ce	45.1	39.6		30.8		48.7				
Pr	6.1	5.3		4.1		6.5				
Nd	25.5	22.4		17.5		27.1				
Sm	5.3	4.8		3.9		5.7				
Eu	2	1.7		1.3		1.8				
Gd	5.1	4.5		3.6		5.3				
Tb	0.7	0.7		0.6		0.8				
Dy	3.8	3.7		3		4.4				
Ho	0.7	0.7		0.6		0.8				
Er	1.6	1.8		1.5		2.2				
Tm	0.2	0.3		0.2		0.3				
Yb	1.2	1.5		1.3		1.7				
Lu	0.2	0.2		0.2		0.3				

Lava flows: BM1, BM2, BM3, BM5, and BM6; dikes: BM9 and BMF; and sills: BM4, BM7, and BM8.

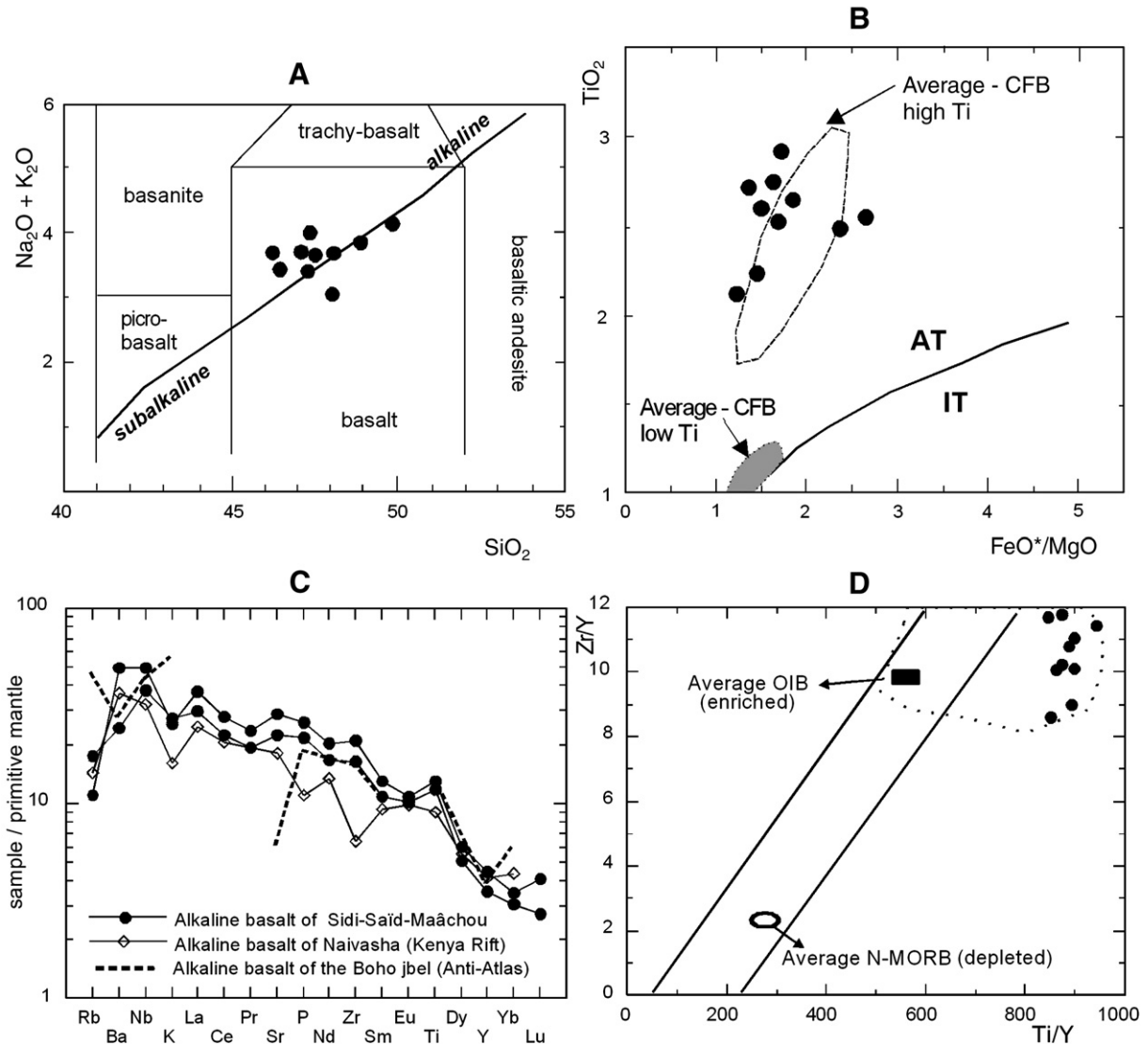


Fig. 3. A. Total alkalis versus silica for the Sidi-Saïd-Mâachou basalts rocks (TAS); plot-fields for volcanic rocks from Le Maitre et al., 1989; the alkaline/subalkaline boundary is from Irvine and Baragar (1971). B. Projection of the Sidi-Saïd-Mâachou basalts rocks in the TiO_2 – FeO^*/MgO diagram (Bébien, 1980); IT and AT — Isotitaniferous/orogenic and anisotitaniferous/anorogenic fields rocks; FeO^* : total iron; CFB field from Albarède (1992) and Deckart et al. (2005). C. Incompatible trace element abundances (normalized to primitive mantle values; Sun and McDonough, 1989) of representative middle Cambrian basalts from Sidi-Saïd-Mâachou. D. Projection of the Sidi-Saïd-Mâachou basalt in the Zr/Y versus Ti/Y diagram (Crowley et al., 2000).

suggests a source related to an enriched mantle-melting zone. Thus, the geochemical signature of the original magmatic liquid would be explained by: (i) melting of an anomalous mantle source, previously contaminated by the assimilation of crustal fragments (Crowley et al., 2000); or (ii) crustal contamination of the original magmatic liquid during its ascent from a deep mantle source (Etxebarria et al., 2006). These processes commonly reflect the degree of extension in continental rifts, as pointed out by several authors (e.g., Furman, 1995, 2007; Le Roex et al., 2001).

4. Sedimentary facies associations, geometrical relationships, and biodiversity patterns

The Sidi-Saïd-Mâachou volcanosedimentary complex is also characterized by the presence of discrete volcaniclastic and

calcarenitic, low-relief sheets and lenses, embedded in green and purple, homogeneous greywackes. These are described below.

4.1. Volcaniclastic lenses

Volcaniclastic breccia and conglomerate lenses, up to 0.6 m thick, show a distinct upward and lateral decrease in volcaniclastic content. The lava flow/volcaniclastic contact is sharp and somewhat erosive, whereas the contact of the volcaniclastic-rich rocks with the overlying greywackes is gradual. Clast-supported, monomictic conglomerate contains subrounded granule to pebble clasts within a volcaniclastic sandy matrix. By contrast, local breccia channels consist of angular, clast-rotated feric granules and boulders embedded in a finer jigsaw-fit and clast-rotated sandy matrix. Feric, feldspar and shard

clasts are the main components of the lenses, and show variable replacements by chlorite, iron oxide, and calcite.

The volcanioclastic breccia and conglomerate were clearly derived from the underlying and lateral lava flows. Coarse breccia appears not to have been transported more than a few metres and is interpreted as autobreccia.

4.2. Volcanioclastic skeletal sheets

A distinct lens-shaped calcarenite body, up to 1.2 m thick, extends across the entire Sidi-Moul-Nker jbel and pinches out radially, disappearing in less than 500 m. The lenticular body can be subdivided into subunits or sheets, less than 0.6 m thick, and bounded by nearly horizontal erosive surfaces. These are commonly covered with either lag deposits or stromatolitic mats. The lag deposits are less than 5 cm thick, their internal fabric is disorganized, and contain siliciclastic (mainly quartz, siltstone, claystone, and volcanogenic debris) and intraformational limestone-dominated clasts. Granule-sized clasts are predominantly angular in shape, whereas smaller clasts are subangular to subrounded. The stromatolitic mats, up to 30 cm thick, display flat, crinkled and domal structures and will be described in detail in Section 4.3.

The upper part of each individual sheet consists of structureless to laminated volcanioclastic packstone. Its skeletal content becomes finer with increasing distance from the thickest beds at the Sidi-Moul-Nker jbel. The sheets contain disarticulated to broken trilobite sclerites, echinoderm ossicles, phosphate- and calcite-walled brachiopods, chancelloriid sclerites, and subsidiary sponge spicules, hyoliths and other skeletonized microfossils (Fig. 4A–B). Skeletal remains are typically randomly oriented, although they are locally preserved with their long axes oriented subparallel to bedding. The volcanioclastic silt to gravel grains, subrounded to subangular in shape, are chaotically oriented. The micritic matrix, where present, contains mixtures of calcite micrite and microsparite, detrital dolomitic and terrigenous silt and sand in variable proportions. It occurs in scattered pockets and lenses (up to 1 cm long) commonly inclined at various angles to bedding, and forming in some cases intraparticular geopetal structures discordant with shelter fillings and stratification.

The volcanioclastic calcarenites were related to washing and polyphase reworking of skeletons and other allochems from the surrounding seafloor. Intraclasts indicate reworking of a partially lithified carbonate seafloor. Such activity probably generated low-angle shoals under high-energy conditions, which were amalgamated vertically over repeated episodes of high-energy deposition. The greatest production of skeletal sediment was yielded from multi-element shelly metazoans that disintegrated after death into their constitutive parts. The bioclasts

display signs of mechanical breakage with many rounded and polished contours. The post-mortem transport of hard parts is indicated by the preservation of shells with exotic (allochthonous) matrix adhered to them or selective replacement by iron-oxyhydroxides. Relic (ferruginous) particles are easily distinguishable by their rusty appearance, ranging from brownish to reddish in colour (Fig. 4A–B). The fossil assemblages appear to be paraautochthonous to allochthonous, and are commingled with locally reworked (polyphase) elements. Much of the sediment was generated from non-reefal pelmatozoan–sponge communities (*sensu* Álvaro and Vennin, 1997).

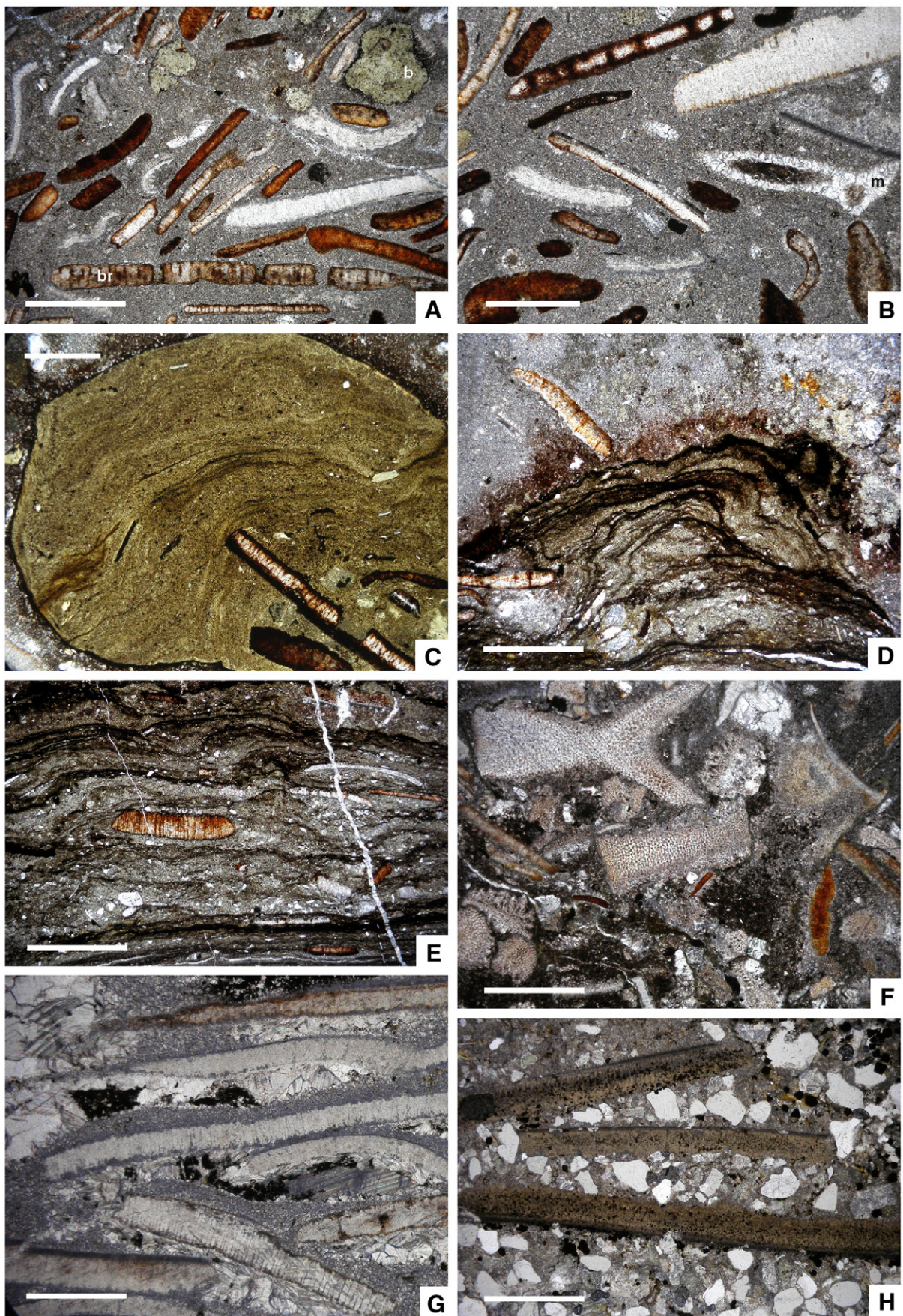
Generation of a powerful, continual water flow by wind and/or swell waves favoured skeletal sediment movement, causing centripetal/radial progradation of sand sheets. Episodic changes in hydrodynamic conditions are indicated by the presence of centimetre-thick stromatolites bounding each individual sheet. The growth of microbial mats is useful here to identify stratigraphic diastems interrupting high-energy clastic sediments (like in the Brèche à *Micmacca* of the High Atlas and Anti-Atlas; Álvaro and Clausen, 2005, 2006, *in press*). The shell concentrations were deposited on a substrate where some intervals of non-deposition (or extremely low-sedimentation rates), which favoured development of microbial crusts, alternated with high-energy sedimentary events. In addition, each shell layer can be considered as a composite event, low-relief shoal complex. These units can be considered as ‘hiatal accumulations’ (*sensu* Kidwell, 1991; Kidwell and Bosence, 1991) because of their subdivision by minor discontinuities or hiatal surfaces (Hillgärtner, 1998), and in view of the composite multi-event nature of the skeletal bodies.

4.3. Microbial mats

Microbial mats form crusts underlying and interbedded within the aforementioned volcanioclastic skeletal sheets. They are up to 12 cm thick and can be followed more than 10 m laterally. The morphology of the lamination does not vary significantly, ranging upward from slightly undulose and wrinkled to domal. The stromatolites are made up of alternating laminae of darker micrite and lighter microsparite with occasional occurrence of peloids and skeletal debris. Well-defined light–dark microlaminae occur locally defined by thin (50–200 µm), gently curved micritic layers.

The microbial mats grew perpendicularly to substrate surfaces, and generally followed their inherited irregularities. High-energy pulses are episodically recorded as scouring surfaces eroding both intra-stromatolitic laminae and stromatolitic tops, subsequently covered by a millimetre-thick calcarenite locally bearing volcanioclastic debris and stromatoclasts (Fig. 4C), and patchy cemented by goethite and hematite. The top of each

Fig. 4. Photomicrographs of the impure limestones from Sidi-Said-Maâchou under parallel light. A–B. Calcareous sheet showing selective ferruginization of polyphase clasts embedded in a micritic matrix; b — basalt clast, t — trilobite sclerite, br — calcite-walled brachiopod valve, m — calcite mosaic; scales = 350 µm and 250 µm, respectively. C. Reworked stromatoclast containing skeletons; scale = 200 µm. D. Onlapping geometry of successive microbial mats forming a dome-shaped growth; scale = 250 µm. E. Detail of the base of a microbial mat showing skeletons and silt embedded in the microbial laminae; scale = 250 µm. F. Argillaceous limestone rich in echinoderm ossicles; scale = 500 µm. G. Detail of sheltered cement mosaics; scale = 500 µm. H. Calcareous trilobite-rich tempestite displaying iron-oxyhydroxide cements dispersed both in the matrix and within the bioclasts; scale = 500 µm.



stromatolitic crust is truncated and covered by either a sheet cavity (described in Section 4.9) or another volcaniclastic skeletal sheet.

Fine skeletal debris and silt washed on to the microbial surface became trapped and bound by the microbial communities in a manner analogous to many modern microbial mats generating ‘agglutinated stromatolites’ (*sensu* Riding, 1999). Sediment consisting of quartz, feldspar, mica, volcaniclastic sand- and silt-sized grains, and skeletons (mainly trilobites and echinoderm ossicles) was episodically trapped and bound into the microbial surface (Fig. 4D–E). Along one lamina, the grains concentrated in small areas outlining micritic masses with a certain relief surrounded by clastic pockets. Although it was introduced or reworked intermittently, by current or wave action, the silt and sand content of the water was not sufficient to prevent the growth of microbial communities.

The first colonization phase of microbial laminated mats lacking embedded siliciclastic material suggests that these substrates were temporarily exposed to quiet water conditions where thin microbial mats covered the substrates. These mats buried a variety of inherited microreliefs related to the irregularities of the shelled substrate. Smooth mats are common in areas of low hydraulic energy (Gerdes and Krumbein, 1994), although a rapid syngenetic cementation allows microbial mats to withstand erosive forces in high-energy environments. We found no evidence of general subaerial exposure and desiccation of these microbial mats. Subsequent winnowing and partial reworking of the substrate (as suggested by the abundance of polyphase clasts and stromatoclasts) would have favoured the formation of irregularities on the substrate that would have induced the instability of lateral early-lithified microbial crusts.

4.4. Reddish argillaceous limestones

The aforementioned volcaniclastic skeletal sheet is unconformably overlain by another lenticular sheet: the reddish argillaceous limestone reaches a maximum horizontal extent of 6 km, is up to 1.2 m thick, and shows lateral transitions to reddish shales bearing centimetre-thick, limestone nodules paralleling stratification. Although there is an upsection increase of shale interbeds, the top of the mudstone–wackestone limestone is sharp. Multi-element skeletons are disarticulated to partly articulated, and local truncating surfaces overlain by grading structures are observable. The limestones display clay-rich packstone and wackestone textures, which are commonly well bedded on a centimetre scale, and contain abundant echinoderm ossicles (Fig. 4F), and subsidiary trilobites, calcite-walled and linguliformean brachiopods, hyoliths, and other undeterminable skeletonized microfossils.

These limestones represent deposition on relatively turbid-water conditions, subject to increased inputs of clay and silt. They were episodically affected by energetic pulses and finally drowned during sea-level rise, because they could not keep up with the rate at which sea level was rising. Less skeletal breakage, associated with the inferred calmer depositional environments, resulted in greater volumes of primary shelter voids afforded by skeletal supports (Fig. 4G).

4.5. Packstone–wackestone bed and nodule calcarenites

They consist of calcarenitic beds and nodules, up to 0.4 m thick, displaying internal anastomosing swarms of clay seams, up to 1 cm thick. The sandy to silty limestone consists of well bedded to nodular packstone and wackestone units rich in the same skeletal components than those described above (Fig. 4H). Locally, centimetre-thick grading units are recognisable, which rest upon sharp truncating bases, in some cases displaying gutter and tool marks. Volcanogenic (femic and feldspar) clasts, sand- to granule-sized, are irregularly distributed. Non-figurative burrowing is locally abundant.

The presence of fragmented bioclasts and graded units, with erosive basal contacts, indicates that the substrate was episodically affected with energetic pulses, likely related to either storm or volcanic eruptions. The presence of bioturbation, dominated by infaunal deposit feeders, allows us to infer that benthic colonization of the seafloor was not inhibited by syn-sedimentary or early-diagenetic cementation.

4.6. Greywackes and interbedded tuffites

This facies association is greenish below and purple above the aforementioned limestone units. It includes massive to planar laminated greywackes and shales. Laminae range from <1 to 4 mm thick and show common grading, which contrasts with the alternation of massive claystone-dominated units, up to 20 cm thick. Basal laminae contacts are commonly scoured and irregular, and flame structures may be present, whereas upper contacts with massive units are generally sharp and planar. Soft-sediment deformation structures, including centimetre- to decimetre-scale convolution and slumping, are common. Horizontal burrows, represented by *Planolites* and *Phycodes*, are common at the top of graded units and on massive claystone beds.

Petrographically, the greywackes contain dominant quartz-feldspathic and subsidiary volcanicogenic and hematite grains. These are set in a matrix rich in mica flakes, chlorite, and sericite. Patches of sparry calcite and dolomite are randomly distributed, generally in amounts of 0–30% of the bulk rock.

The upper purple unit (Fig. 2) contains centimetre-thick tuffites, recognisable by their basal truncating contacts and upward grading, common rip-up shale clasts forming basal lags, and pinkish colour of their scattered euhedral K-feldspar phenocrysts embedded in a clayey matrix. Faint lamination, with sharp contacts, and both normal and inverse grading is present. The tuffs contain <1 cm-sized euhedral quartz and feldspar phenocrysts embedded in a fine-grained microcrystalline quartz-rich matrix.

The facies association represents deposition from suspension under low-energy, tranquil-water conditions, episodically punctuated by low-concentration turbidity currents. Bouma sequence divisions T_d and T_e (Bouma, 1960) are recognisable in the greywackes. Although the background deposition took place in relatively deep-water substrates, they recorded normal oxygenated conditions, as indicated by the abundance of horizontal burrows. The onset of interbedded tuffites reflects the influence of neighbouring acidic volcanism.

4.7. Palaeoenvironments and geometrical relationships

As described above, the Sidi-Saïd-Maâchou volcanosedimentary complex displays a lenticular shape, up to 10 km across and *ca.* 16 m thick. The complex is embedded in a thick and homogeneous, turbiditic succession dominated by greywackes and shales. The two limestone-dominated facies associations of the complex, named volcaniclastic skeletal sheets and reddish argillaceous limestones, display similar geometries: low-relief tabular or sheet-like bodies, up to 1.2 m thick, *ca.* 10 km wide, and stacked in a vertical fashion. Their sheet margins laterally intercalate with shales and greywackes by thinning away from the thickest crest (at Sidi-Moul-Nker jbel, where the log was measured; Fig. 2). The sheet limestones pass laterally into centimetre-thick, bioclastic and intraclastic limestones and dolostones, alternating with greywackes and shales containing scattered skeletons. The presence of larger shell fragments adhered to margins of some scattered intraclasts suggests that the sediment was partly lithified when it was reworked. Individual sheets were influenced by the local hydrodynamic regime: although the shelled accumulations were sufficiently coherent to withstand fairly turbulent conditions, they were nonetheless subject to periodic erosion, as witnessed by the

abundance of lithified intraclasts dispersed in laterally equivalent, greywacke strata. As illustrated in Fig. 2, at least two lava flows are capped with limestone sheets, whereas the reddish argillaceous limestone was subsequently eroded (see a channelized contact in Fig. 5A) by another lava flow. This again points to an early lithification of the carbonate substrates.

Development of shelled concentrations in this palaeogeographically restricted area appears to have been constrained by some particular environmental conditions of reduced clastic influence, a critical combination of turbulence and clear waters, and an irregular substrate controlled by the onset of basic lava flows of reduced topographic relief. Carbonate productivity was localized on substrates capping volcanic effusion.

There is a significant hiatus in the timing of deposition between both carbonate units. The top of the underlying volcaniclastic skeletal sheet is an ironstone bed, up to 10 cm thick, where goethite occurs as thin ferruginous-impregnated litho- and bioclasts, and crystals occluding primary porosity, finally capped by laminated bands, less than 1 cm thick, containing ‘floating’ litho- and bioclasts (Fig. 5B). The progressive lithification of this hardground was marked by the presence of burrows characteristic of firm substrates: the top of the hardground shows the presence of *Arenicolites*, *Diplocraterion*, and

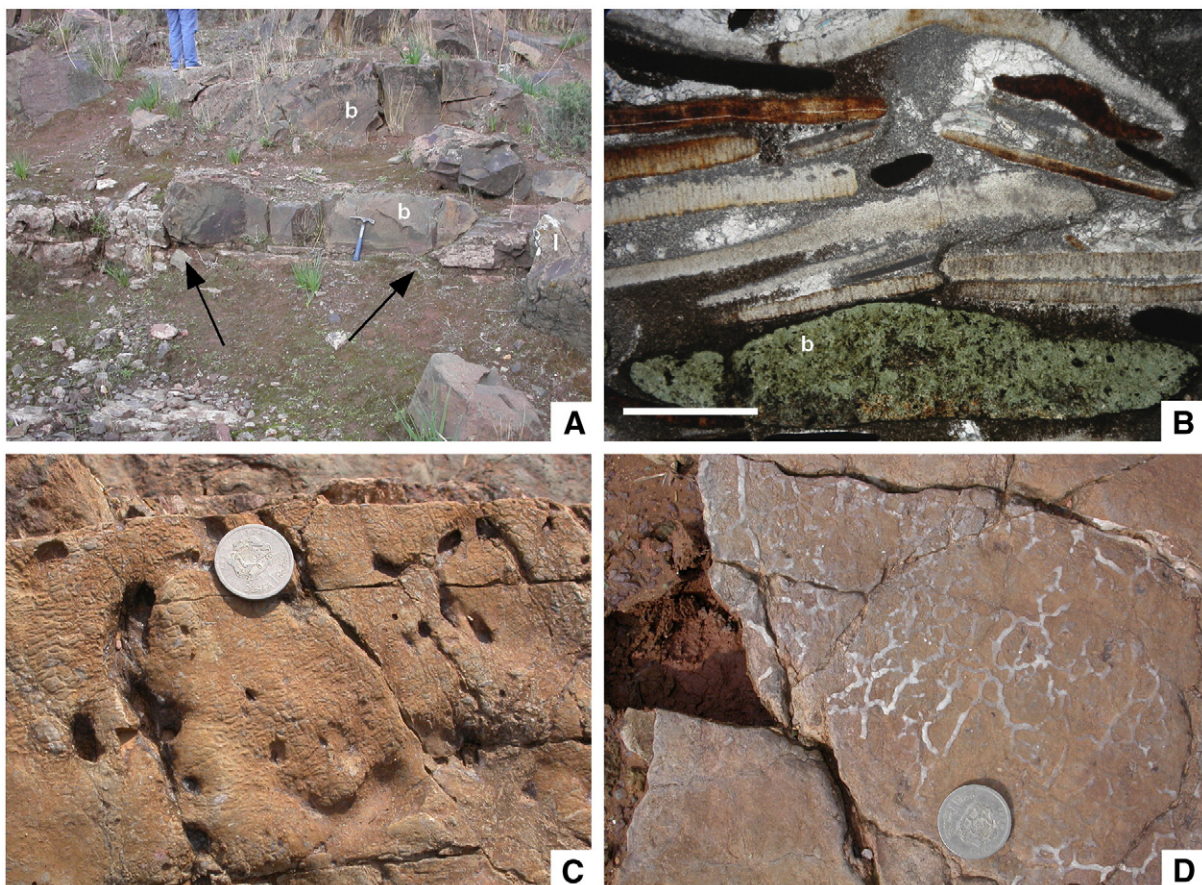


Fig. 5. A. Lava channel (b) eroding the argillaceous limestone (li) described in the text; erosive contact marked with arrows. B. Photomicrograph of the hardground horizon showing the mixture of skeletons (mainly trilobite sclerites) and basalt clasts (b) embedded in a micritic matrix partly replaced by iron-oxyhydroxide cements; scale=500 µm. C. Top of the hardground infested with *Arenicolites* burrows; scale=2 cm. D. Another surface of the hardground with *Thalassinoides*-like networks; scale=2 cm.

Thalassinoides-like burrow networks (Fig. 5C–D), the porosity of which is wholly occluded with goethite cements. Evidence for subaerial exposure is absent.

After an indeterminate hiatus, carbonate productivity renewed in a deeper environment. The deposition of reddish limestones was terminated either by flooding and/or the progressive influx of argillaceous sediment that poisoned carbonate production. The final demise of this short-lived carbonate platform was related to a combination of tectonic activity in the immediate vicinity of the platform.

4.8. Biodiversity patterns of shelly benthic communities

Echinoderm ossicles, trilobites and linguliformean brachiopods are the most abundant contributors to the skeletal fraction of limestones. Sampled trilobite debris is highly fragmented, which dramatically precludes any systematic determination. However, in order to test the biodiversity patterns displayed by other taxa, we extracted from the limestones of the Sidi-Saïd-Mâachou volcanosedimentary complex acid-resistant skeletons, by dissolving the rock in a dilute (10% by volume) acetic acid solution. Two limestone beds yielded linguliformean brachi-

pods. The volcanoclastic skeletal sheet SM5 (see Fig. 2), which caps a lava flow, has yielded two species: *Almahadella braunae* Streng, 1999 and *Eothele* sp. cf. *E. spurri* (Walcott, 1908) (Fig. 6). The former is endemic from Morocco, and was described by Streng (1999) from the *Ornamentaspis frequens* Zone (middle Cambrian; Geyer and Landing, 1995) of the High Atlas. Recently, *Almahadella braunae* has also been reported from the middle Cambrian Týřovice Greywacke of Bohemia (Mergl and Kordule, 2008). *Eothele spurri* is present in the *Bonnia-Olenellus* Zone (Combined Metals Member of Pioche Shale) of Nevada, and was not so far reported in Morocco. There are some similar shells described by Mergl (1988) from the middle Cambrian of Bohemia as *Botsfordia epigona* Mergl; these shells in reality belong to *Karathele*. The overlying reddish argillaceous limestone of level SM12 has only yielded acrotretid dorsal valves, which precludes any systematic determination due to the necessity of studying ventral valves.

Despite the difficulty in taxonomically determining highly fragmented trilobite and brachiopod debris, we can conclude that the biodiversity patterns recorded in the limestones of Sidi-Saïd-Mâachou are similar to those recorded in other volcanoclastic limestones of the Anti-Atlas, such as the Brèche à

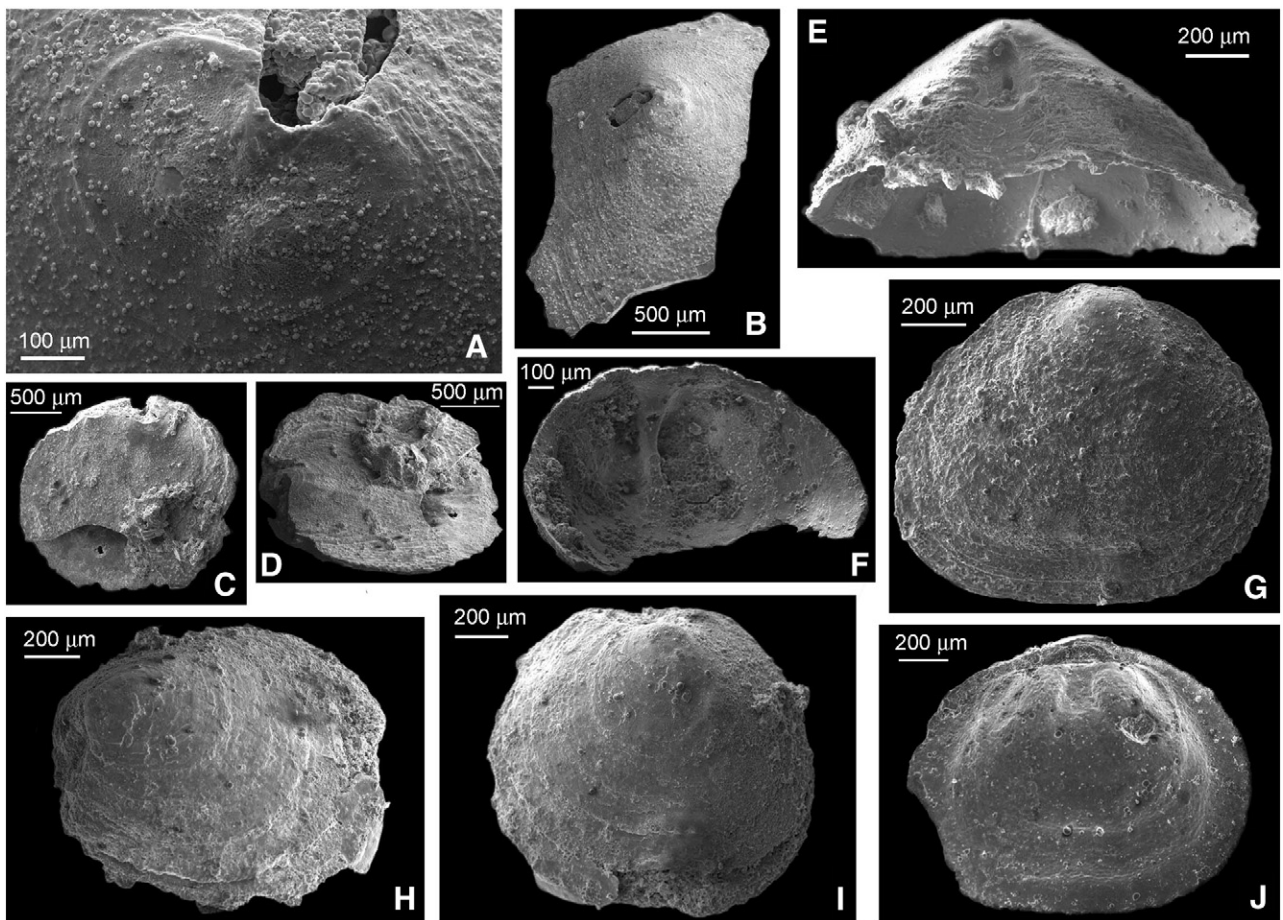


Fig. 6. Characteristic linguliformean brachiopods of the Sidi-Saïd-Mâachou volcanosedimentary complex. A–D, *Eothele* sp. cf. *E. spurri* (Walcott, 1908); A–B, NMW 2007.54G.1, pitted larval shell and oblique lateral view of incomplete ventral valve; C–D, NMW 2007.54G.2, dorsal and oblique lateral dorsal views of conjoined valves. E–J, *Almahadella braunae* Streng, 1999; A, NMW 2007.54G.3, posterior view of ventral valve showing pedicle foramen; F, NMW 2007.54G.4, ventral valve interior showing ridge-like apical process; G, NMW 2007.54G.5, dorsal valve exterior; H–I, NMW 2007.54G.6, ventral valve oblique lateral view and exterior; J, NMW 2007.54G.7, dorsal valve interior. NMW: National Museum of Wales.

Micmacca Member of the Jbel Wawrmast Formation (Geyer and Landing, 1995; Streng, 1999). Therefore, the studied limestones do not represent any restricted palaeoenvironment, related to anoxic vent conditions and typically colonized by monospecific opportunistic taxa (Van Dover, 2000).

4.9. Post-sedimentary development of sheet cavities

The aforementioned volcaniclastic skeletal sheets contain interbedded subhorizontal sheet cavities that either contain relics of microbial mats or change laterally into them. The sheet cavities range from 1 to 30 cm in thickness and can be followed laterally up to 4 m. The floors generally do not deviate more than 20° from the stratification plane, whereas the roofs are generally irregular to undulate (Fig. 7A–B). Although the roofs are commonly unsupported by skeletons, skeletal fragments can be found hanging from the roofs, and either project into the cavities (as isolated protruding skeletons; Fig. 7C) or separate lateral cavities (Fig. 7D).

The cavities are filled with internal sediment and calcite cements. The internal sediment consists of alternating medium-to low-angle, micritic and calcarenous laminations, up to 2 mm thick, locally displaying onlapping geometries. The calcarenous and micritic laminae are bounded by sharp contacts. The former are rich in skeletons, which can protrude into the underlying micritic lamination, quartzofeldspathic grains, and goethitic

clasts and cements. The latter are less abundant and dispersed in the micritic laminae.

Two generations of calcite cements occluded the remaining geopetal space: a first-generation, isopachous, inclusion-rich calcite cement, and a second generation, clean, blocky, calcite cement. The fibrous cloudy calcite cement also occurs as rinds around skeletons floating within the internal sediment (Fig. 7C). The fibrous cement is not radial, and crystals are characterized by sweeping extinction under crossed nicols. These thin layers commonly range from 10 µm to 2 mm in thickness. The second and most abundant cement, in the cavities that are not completely occluded with fibrous calcite, is blocky calcite cement. Its layers, up to 2 cm thick, are composed of variably elongate to obtuse, dendate calcite crystals that nucleated on pre-existing fibrous crystals.

Three steps are necessary to understand the origin and occlusion of these sheet cavities:

- (i) The formation of sheet cavities in unconsolidated carbonate beds of microbial origin, interbedded with volcaniclastic skeletal sheets, by post-depositional decay of (partly preserved) microbial mats.
- (ii) The original morphology of sheet cavities was subsequently modified by both through-flowing marine pore waters, causing internal erosion and sedimentation below the sediment–water interface, and gravitational collapse

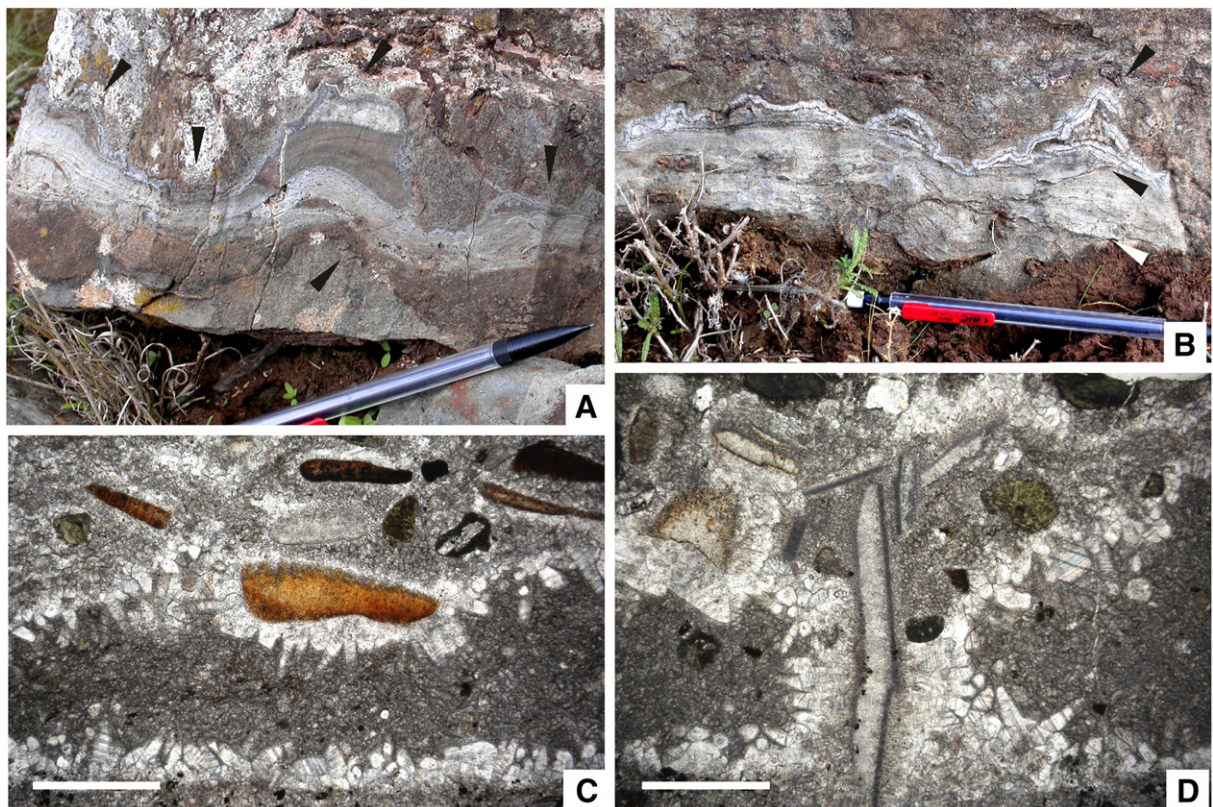


Fig. 7. Field aspect and photomicrographs of the sheet cavities. A. Sheet cavity with undulating base and top, where the darker laminated infill is overlain with lighter geopetal cements. B. Sheet cavity with flat base and irregular ceiling. C. Thin-section photomicrograph, with parallel light, showing a millimetre-scale cavity with fibrous cements encrusting micrite and skeletal walls located at the base and ceiling of the cavities; scale=2 mm. D. Junction between two lateral sheet cavities separated by a trilobite sclerite; scale=2 mm.

of unconsolidated sediment from the roof sand walls of the cavities (see, e.g., Wallace, 1987). As a result, the roof and floor of the cavities probably migrated upward through the sediment. The cavities were capable of migrating upward leading a trail of internal sediment beneath. In some cases, the migrating cavities were trapped beneath skeletal constituents, forming diagenetic ‘shelter’ cavities: when the cavities are partly ‘sheltered’ by trilobite sclerites and brachiopod valves they show no evidence of collapse or erosion.

- (iii) As sedimentation proceeded above, more deeply buried cavities were subjected to a decrease in the velocity of through-flowing water. Eventually, the velocity of water was reduced to a point where no further erosion took place. As a result, the cavities began their occlusion by two processes: internal sedimentation and calcite precipitation. After partial infill of the cavities by internal polyphase sedimentation, these were still connected to the surface allowing an active circulation of marine pore waters through them responsible of cement occlusion. The precipitation of calcite cement within the cavities and the lithification of the surrounding carbonate mud would have eventually stabilized the cavities.

The sheet cavities of Sidi-Saïd-Mâachou resulted from a process of internal erosion and sedimentation (internal reworking), which occurred directly below the sediment/water interface. They mimic the morphology and infill of stromatactis and zebra rocks (Bosence and Bridges, 1995; Flügel, 2004; and references therein). Both structures may display a simple cement fill or complex banding of cement and internal sediment. As in the case of the sheet cavities described in this paper, some isolated stromatactis and zebra swarms originated via decomposition of microbial mats and soft-bodied organisms, such as sponges, non-skeletal algae and bryozoans (Demicco and Hardie, 1994; and references therein).

In order to identify the carbon source and the carbonate-forming mechanism for the calcite infill and cements that occluded the sheet cavities, carbon and oxygen isotope analyses were carried out on the aforementioned textures (Table 2). The individual components were removed by dental drill under a binocular microscope and the powdered samples were digested in 100% phosphoric acid at 25 °C. The resulting CO₂ gas was analyzed using an ISOPRIME mass-spectrometer for isotopic analysis at the Salamanca University, Spain (for details, see Al-Assam et al., 1990). The isotopic composition of calcite is expressed by the conventional δ notation relative to the V-PDB reference; $\delta = [(Rs/Rr) - 1] * 1000$, where $R = ^{18}\text{O}/^{16}\text{O}$ or $^{13}\text{C}/^{12}\text{C}$ respectively in the sample and in the reference. Analytical reproducibility (1σ) is 0.1‰ for $\delta^{18}\text{O}$ and $\delta^{13}\text{C}_{\text{carb}}$.

The results from analysis of the internal sediment and the fibrous and blocky cements indicate that the whole infill has a similar $\delta^{13}\text{C}_{\text{carb}}$ signature, distinctly different from the $\delta^{13}\text{C}$ values exhibited by the host-rock (matrix of the volcanic-lastic skeletal sheets). The cavity infill yielded ratios between −10.95‰ and −17.12‰ $\delta^{13}\text{C}_{\text{carb}}$ and −9.88 and −16.02 $\delta^{18}\text{O}$, and the host-rock −5.27‰ and −16.2‰, respectively.

Table 2
Carbon and oxygen isotope data from the sheet cavities

	$\delta^{13}\text{C}_{\text{carb}} \text{‰ PDB}$	$\delta^{18}\text{O}_{\text{carb}} \text{‰ PDB}$
Host rock	−5.27	−16.5
	−5.02	−16.7
	−6.12	−17.03
	−5.71	−17.56
Microbial mat	−12.93	−14.21
	−15.07	−9.98
	−15.87	−14.86
	−16.21	−12.77
Sediment infill	−10.95	−14.75
	−17.12	−16.02
	−14.36	−13.21
	−14.73	−15.52
Fibrous cement	−12.29	−12.56
	−14.47	−11.92
	−13.76	−14.98
	−10.36	−15.31
Blocky cement	−11.49	−9.88
	−14.61	−9.71
	−13.72	−11.98
	−13.41	−14.66

Similar analyses of $\delta^{18}\text{O}$ compiled from Cambrian tropical low-Mg calcite-walled brachiopods (probably yielding the closer proxy to real seawater chemistry) vary from −7 to −12‰ (Wadleigh and Veizer, 1992). However, this difference must not be exclusively related to diagenetic processes. Bruckschen et al. (1999) pointed out that $\delta^{18}\text{O}$ variations in modern tropical brachiopods at shelf depths are ~4‰ and, for specimens sampled in temperate climates, they span about 8‰. Oxygen isotopic differences can also be triggered with recrystallization of the shell calcite after deposition (Veizer et al., 1996). As an average, the difference between bulk rock and skeletal calcite (e.g., calcite-walled brachiopods) $\delta^{18}\text{O}$ values amounts on average to about 2‰ (Schrag et al., 1995; Veizer et al., 1999). $\delta^{18}\text{O}$ data show similar oscillations that the $\delta^{13}\text{C}$ data; this and their depleted character can be reasonably ascribed to diagenetic alteration. Micritic recrystallization would have caused $\delta^{18}\text{O}$ values to decrease reflecting a diagenetic resetting and post-depositional alteration of the Sidi-Saïd-Mâachou limestone samples, probably primarily controlled by thermal parameters during sedimentation and burial temperatures.

The analyzed carbon-isotope values are not consistent with those expected for Cambrian seawater. $\delta^{13}\text{C}_{\text{carb}}$ values are also depleted by comparison with the background $\delta^{13}\text{C}_{\text{carb}}$ values analyzed in Cambrian tropical brachiopods (ranging from −2.2 to +1.0‰; Wadleigh and Veizer, 1992). In our case study, primary controls on ^{13}C depletion can be related to two factors: the proportion of oxidized kerogen incorporated in the host limestone (Schumacher, 1996) and diagenesis; other factors, such as the influence of riverine carbon in nearshore environments (Koch et al., 1992) and interaction with $\delta^{13}\text{C}$ -depleted methane (−40‰ to −74‰; Mazzini et al., 2004), are not significant. The carbon-isotope value of marine organic matter is about 9–15‰ more negative than inorganic bicarbonate (Marshall, 1992; Walter et al., 2007); they can reach a minimum of −26.3‰ in the case of algal matter degradation (Lehman

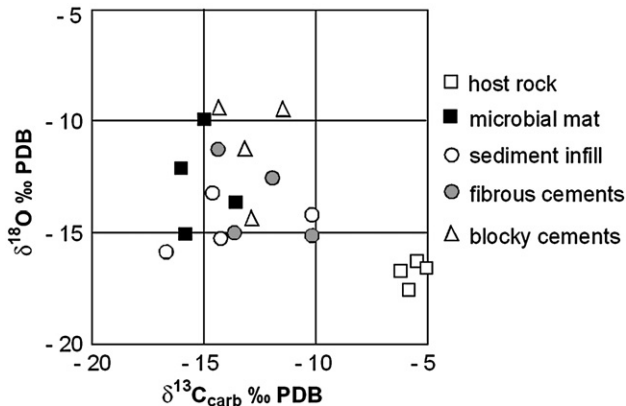


Fig. 8. $\delta^{18}\text{O}$ versus $\delta^{13}\text{C}_{\text{carb}}$ crossplot of the data reported in Table 2.

et al., 2002). Thus, degradation of organic matter has the potential to significantly alter the carbon-isotope composition of marine carbonate sediment (Glumac and Walker, 1998).

The wide variability of $\delta^{18}\text{O}$ values and lack of covariance between $\delta^{13}\text{C}$ and $\delta^{18}\text{O}$ values (coefficient of correlation $r^2=0.209$; Fig. 8) suggest that the studied limestones were not significantly submitted neither to meteoric nor to marine-meteoric waters of the mixing zone (Allen and Matthews, 1982). As a result, despite the depleted character of the ^{18}O and ^{13}C values, the lack of $\delta^{13}\text{C}_{\text{carb}}/\delta^{18}\text{O}$ covariance suggests a similar diagenetic behaviour for all the samples. Although the

absolute isotopic values were probably depleted by hydrothermally enhanced and burial temperature, they were affected in a similar way throughout the whole textures. This allows us to interpret the sharp difference in $\delta^{13}\text{C}_{\text{carb}}$ yielded by the host-rock micritic matrix and the (sedimentary and cement) infill (-5.1‰ to -5.4‰ versus -10.95‰ to -17.12‰) as a direct influence of the degradation of the microbial mats responsible of the sheet-cavity formation.

4.10. Metalliferous precipitates

A variety of polymetallic mineralizations are hosted in the impure limestones of the Sidi-Saïd-Mâchou volcanosedimentary complex. They were characterized using a combination of methods, including transmitted light microscopy and scanning electron microscopy operating in back-scattered electron image and EDS analysis. SEM analysis was made by using a JEOL JSM-6400 fitted with an Oxford Instruments D6679 detector. Back-scattered (BSE) imaging and energy-dispersive X-ray (EDS) analyses were obtained by SEM with the following measurement conditions: accelerating voltage 20 kV, beam current 1–2 nÅ, and a counting interval of 50 s. Analytical results display an error of $\pm 5\text{--}7\%$.

The calcarenitic limestones display, at least, five major early-diagenetic porosity-occluding cementation phases, all of them affected by stylolite-related fracturing. Two early-diagenetic phases of cementation are subsequently distinguishable, the

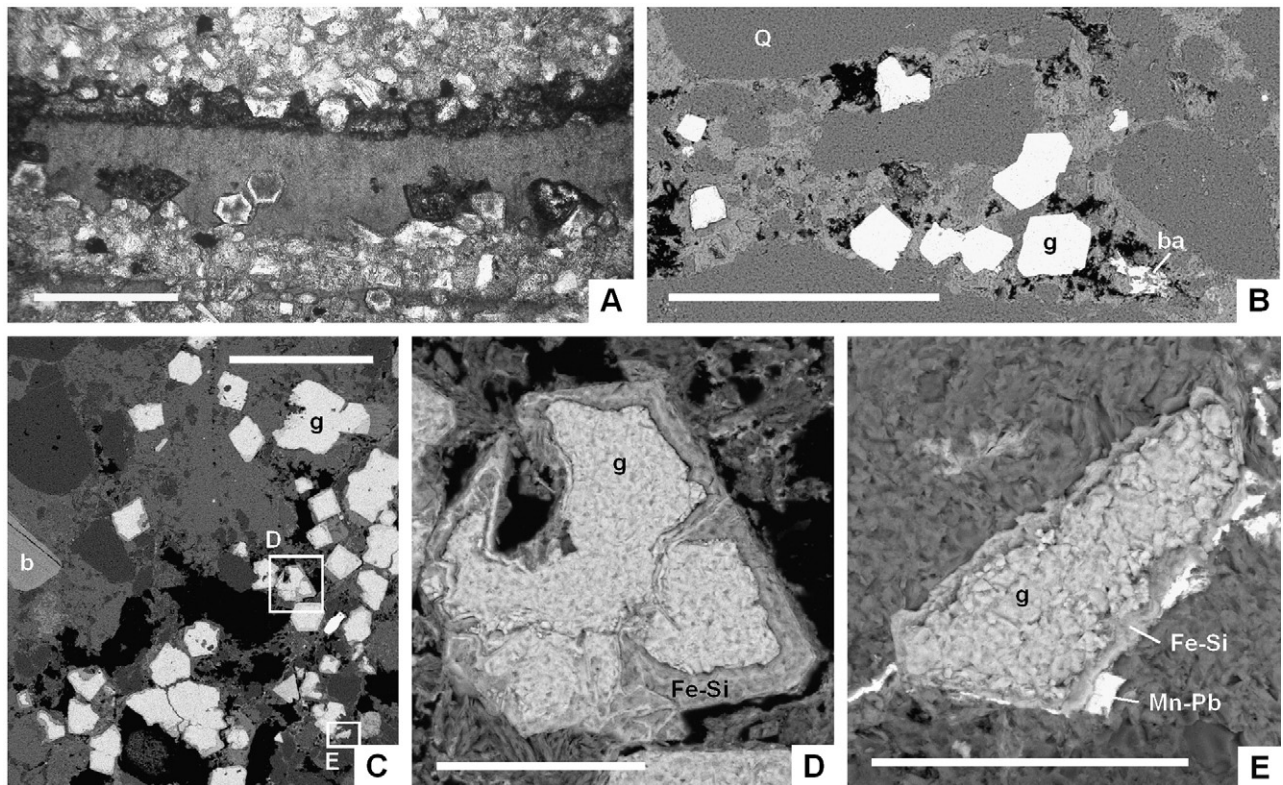


Fig. 9. A. Authigenic K-feldspar crystals growing along the margin and within a trilobite sclerite; scale = 2 mm. B–E. Back-scattered electron micrographs of several oxyhydroxide crystals. B–C. Goethite crystals embedded in a quartz-rich calcarenite; scales = 200 μm and 400 μm , respectively. D–E. Zonation of amorphous oxyhydroxides around a goethite nucleus (crystals boxed in Fig. 9C); scales = 50 μm ; b — phosphate-walled brachiopod, ba — barite g — goethite, Fe–Si, iron–silica oxyhydroxide, Mn–Pb, manganese–lead oxyhydroxide, Q — quartz.

separation of which is marked by partial dissolution (evidenced by the presence of solution vugs). The first phase of diagenetic cementation spanned precipitation of authigenic feldspar and barite, partly altered and replaced by fibrous clays. The K-feldspar crystals are mostly turbid and show signs of diagenetic precipitation, dissolution, and partial albitionization. They are specially concentrated along trilobite and calcite-walled brachiopod skeletons (Fig. 9A). By contrast, barite precipitation dominantly occurs as tabular and prismatic forms that seem to have crystallized in the primary pore spaces of both the calcite micrite and clayey matrix (Fig. 9B).

The first early-diagenetic phase was succeeded by a dissolution phase and the formation of a vuggy porosity, which predated three generations of oxyhydroxide precipitation. A BSE analysis enables us to distinguish them as: (i) authigenic goethite crystals, subsequently coated by (ii) Fe–Si amorphous oxyhydroxide and (iii) Mn–Pb amorphous oxyhydroxide rims. The goethite crystals, dominant in volume, occur as botryoidal aggregates, up to 20 µm in size, and euhedral to anhedral (the latter occluding the vuggy porosity) crystals, up to 3 mm in size. They contain more than 90 wt.% of iron-oxyhydroxide mixed with low contents of SiO₂ (Table 3). The following X-ray amorphous oxyhydroxides, up to 20 µm thick, occur both coating the goethite crystals and occluding the remaining porosity (Fig. 9C–D). The Fe–Si amorphous oxyhydroxide differs from the goethite in the iron content, which is lesser in the former (82–89 versus 93–98 wt.%) and contains remarkable quantities of Al₂O₃, MnO and CaO. The final X-ray amorphous (zenzenite-like) Mn–Pb oxyhydroxide is characterized by MnO and PbO contents that exceed 50 and 20 wt.%, respectively, and shows depleted contents of Al₂O₃, MgO, CaO, K₂O, Ti₂O₅, and CoO.

Authigenic K-feldspar crystals are common cements in rift settings (Morad et al., 1989; El Tabakh et al., 1997), and are commonly produced by the reaction of hypersaline–alkaline waters (rich in K) with volcanic ash. The polymetallic mineralizations of Sidi-Saïd-Mâachou, rich in barite and Fe–Mn oxyhydroxides, have remarkable similarities to those of many low-temperature diffuse venting (Hannington et al., 1995; Daesslé et al., 2000), mid-oceanic ridges, island arcs, back-arc basins and hot-spot volcanoes (Glasby et al., 1997; Bognadov

et al., 1998; Marchig et al., 1999). Iron oxyhydroxides commonly form as either replacement of massive sulfides on deep-sea vents (e.g., Lüders et al., 2001) and direct precipitation from hydrothermal solutions (Pichler and Veizer, 1999), although they can also be associated with the alteration of basaltic lavas (Nédelec, pers. commun., 2008). The distinct microscopic zoning exhibited by Fe- and Mn-rich oxyhydroxides can be constrained by temperature (as Mn submarine deposits form usually between 5 and 25 °C; Burgath and von Stackelberg, 1995), and the kinetically limited oxidation of Mn, unlike iron, whose precipitation occurs immediately in oxidizing conditions (Mills et al., 2001).

The onset of partial dissolution pre-dating the precipitation of oxyhydroxides can be related to the input of unsaturated waters. However, it is not easy to discriminate the provenance of these unsaturated waters because they can be related to either meteoric or acidic hydrothermal influence. The widespread development of vuggy porosity and oxyhydroxide precipitation below the aforementioned hardground horizon contrasts with their drastic reduction upsection: the diagenetic processes are still present in the lowermost centimetres of the reddish argillaceous limestones, but disappear upward. As a result, a probable interpretation for the introduction of low pH, oxygen-rich meteoric waters and subsequent dissolution may be related to regional uplift, also responsible of the hardground unconformity that caps the volcanoclastic skeletal sheets.

5. Discussion

5.1. Nucleation and demise of carbonate factories on uplifted rift shoulders

The Sidi-Saïd-Mâachou volcanosedimentary complex is characterized by the interfingering of the aforementioned volcanic and sedimentary rocks. Effusion of submarine lava flows alternated with nucleation of shelly and microbial carbonate factories. Both the geometry and facies of the skeletal calcreneous sheets point to a short-term episode of shallow-water (shoreface) conditions interrupting the general turbiditic claystone and greywacke deposition, more than 1000 m thick, of the middle Cambrian ‘Schistes à Paradoxides’. The stratigraphic ranges of the trilobites and linguliformean brachiopods found in the volcanosedimentary complex (Gigout, 1951: p. 25; and this work) suggest a chronostratigraphic age included within the Caesaraugustan–middle Langueudocian interval (middle Cambrian; Álvaro and Vizcaíno, 1998). This time span is represented in other neighbouring basins of West Gondwana (such as the Anti-Atlas and south-western Europe) by deposition of transgressive shales punctuated by an early Langueudocian regression (see recent revisions in Álvaro et al., 2003, 2007; Álvaro and Clausen, 2005). However, in the Coastal Meseta, the drastic modifications in thickness of the turbiditic-dominated ‘Schistes à Paradoxides’ (Bernardin et al., 1988; Roussel and Bernardin, 1991) suggest the onset of a tectonically controlled subsidence during middle Cambrian times, responsible for the breakdown of the Coastal Meseta platform into palaeohighs and grabens.

Table 3
Chemical composition ranges (in wt.%) of the measured oxyhydroxides

	1st	2nd	3rd
	Goethite crystals	Fe–Si amorphous	Mn–Pb amorphous
SiO ₂	2.3–4.6	7.1–9.7	0.7–9.5
Al ₂ O ₃		1.6–4.3	1.1–6.7
Fe ₂ O ₃	93.7–97.6	82.4–89.4	0–5.5
MnO		0–4.5	49.7–66.9
MgO			0–0.9
CaO	0–1.4	1.4–2.2	1.9–4.0
K ₂ O			0–2.8
TiO ₂			0–1.1
CoO			0–17.7
PbO			20.5–28.5

Each range based on 10 analyses.

The shallowing represented by the volcaniclastic calcarenitic sheet, capped by a hardground, must be related to a forced regression recorded in a reduced palaeogeographic area located at a junction of several graben segments. A possible angular unconformity can be envisaged separating the calcarenitic sheet and the reddish argillaceous limestone, but the contact was probably reactivated as a fault during the Hercynian deformation and cannot be clearly mapped. All these data enables us to interpret the setting of the Sidi-Saïd-Mâachou volcanosedimentary complex as a short-term uplifted area, which leaved recognisable effects on the sedimentation, such as carbonate productivity, localized shoaling, and radial thinning of the strata from the uplifted area. Footwall uplift of fault blocks did not result in subaerial exposure, but possible tilting and a distinct episode of non-deposition and condensation are inferred. The final demise of this ‘short-lived’ episode of carbonate productivity was related to a combination of tectonic activity and flooding of the area.

5.2. A comparison with the Cambrian Brèche à Micmacca of the High Atlas and Anti-Atlas

As pointed out by Gigout (1956), a comparison of the Sidi-Saïd-Mâachou volcanosedimentary complex with the Brèche à *Micmacca* Member (Jbel Wawrmast Formation) of the Anti-Atlas and High Atlas allows a better understanding of the geodynamic control on the shape and size of volcaniclastic shell concentrations. The shell accumulations recorded in the Brèche à *Micmacca* consists of hiatal ‘event concentrations’ of normally dispersed, allochthonous, skeletal and volcanogenic constituents, deposited coevally with a volcanic activity across the lower-middle Cambrian transition (Álvaro and Clausen, 2005, 2006, *in press*), and post-dating a distinct angular unconformity in the Ouriken-n’Ourmast region of the Moroccan Anti-Atlas (the so-called ‘Salaïrian’ tectonic phase of Hupé, 1955). The sharp lateral migrations shown by the shifting-centres of shell accumulation were primarily controlled by changes in seafloor topography accompanied by deposition of K-bentonites and explosive volcanism. The end of uplift movements is marked, on the top of the Brèche à *Micmacca*, by subaerial exposure, microkarstification, and colonization of their karstic cavities by coelobiontic microbial communities (Álvaro and Clausen, 2006). This forced regression, absent in laterally equivalent strata, was also followed by flooding of the palaeotopography and deposition of onlapping offshore shales.

5.3. Tectonic and palaeogeographic implications

The regional uplift of rift shoulders in the Coastal Meseta of Morocco fits well with the extension of carbonate strata, non-voluminous effusion of basaltic flows, shoaling coeval with the onset of the volcanosedimentary complex, and regional palaeogeography (e.g., Van Valen et al., 1995; Kampunzu et al., 1997, 2000; Chaudhuri et al., 2002; Chaudhuri and Deb, 2004; Korme et al., 2004). Since the end of the Pan-African orogeny, an intense volcanism affected the Moroccan margin of West Gondwana as a result of crustal extension with a space-time

migration from the SW (Anti-Atlas) to the NE (High Atlas and Coastal Meseta). Such rift system fragmentation and propagation of the locus of volcanic activity was associated with important changes in the nature of the erupted magmas, ranging from tholeiitic- to alkaline-dominated volcanic rocks. The rift system is considered as an intra-continental ridge system, comprising several SSE–NNW axial rift grabens and subsidiary E–W branches. The shape and size of grabens are mainly deduced by biostratigraphically constrained iso-thickness contours (Bernardin et al., 1988; Piqué et al., 1995; Piqué, 2003; Soulaimani et al., 2003). The middle Cambrian rift envisaged in the Coastal Meseta was segmented into graben troughs, trending SSW–NNE, separated from each other by relative plateaus. One of them, the so-called BHC1-El Arba graben (Bernardin et al., 1988; Fig. 1B), runs SSW–NNE, thins progressively northward, and its northern edge is located in the vicinity of Sidi-Saïd-Mâachou.

The patchy distribution of ‘anomalous’ carbonate factories (taking into account the thick and monotonous turbiditic succession in which the thin carbonate-rich volcanosedimentary complex is embedded), during the lower-middle Cambrian transition in the Anti-Atlas and High Atlas and the Caesaraugustan–middle Languedocian (middle Cambrian) in the Coastal Meseta, coincides with the northward diachronous migration of rifting structures throughout the Moroccan margin of Gondwana. The shallowest rift shoulders were mantled by lenticular, hiatal, shelled concentrations, episodically interrupted by microbial mats. The migration of the loci of carbonate productivity marks the subsequent migration of coeval tectonic and magmatic processes, related to local uplift and tilting. These shell concentrations formed at shallower water depths than did laterally equivalent, carbonate-poor substrata, suggesting development of localized forced (or uplifted) shoalings.

6. Conclusions

During the middle Cambrian, the Moroccan rift that fringed West Gondwana propagated northward and reached the Coastal Meseta. The Sidi-Saïd-Mâachou area represents an anomalous uplifted area of the Coastal Meseta located at the junction of several graben segments, where a basic magma was extruded along fissures or intruded as sills and dikes. Effusion took place under calm conditions and alternated with episodes of carbonate productivity leading to the record of a broad lenticular volcanosedimentary complex, up to 10 km across and *ca.* 16 m thick, embedded in a thick and homogeneous, turbiditic-dominated succession, named regionally the ‘Schistes à *Paradoxides*’. Two main calcarenitic sheets (or shelled accumulations) are recorded, representing a composite shoaling–deepening interval bounded by a significant hiatus, marked by a ferruginous hardground. The identification of a possible angular unconformity at this contact is precluded by its apparent reactivation as an Hercynian fault. Fluctuation in the benthic hydrodynamics favoured the episodic development of microbial mats encrusting the calcarenitic substrates. Degradation of organic matter led to the formation of sheet cavities, up to 30 cm thick, which were subsequently filled by internal sediment and several

phases of calcite cementation. The depleted character of the carbon and oxygen isotope data yielded by the host-rock and infill reflects diagenetic alteration mainly driven by hydrothermal and burial temperatures. Despite this clear influence, the sharp difference in $\delta^{13}\text{C}_{\text{carb}}$ values yielded by the micritic host-rock and the (sedimentary and cement) infill, ranging from 5 to 12‰, suggests a direct influence from the degradation of microbial mats responsible of the formation of sheet cavities. The post-sedimentary influence of metalliferous fluids is also associated with the precipitation of K-feldspar, barite, and three generations of Fe, Fe–Si, and Mn–Pb oxyhydroxides.

The geometry and facies of the skeletal calcarenite sheets, the volcanic influence, and the shoaling character of the loci of carbonate productivity at Sidi-Saïd-Mâachou is comparable to those previously reported across the lower-middle Cambrian transition in the Atlas Mountains, and represented by the hiatal shelled accumulations of the Brèche à *Micmacca*. As a result, we propose that the patchy and diachronous distribution of these ‘anomalous’ carbonate factories, represented by the Brèche à *Micmacca* across the lower-middle Cambrian transition in the Anti-Atlas and High Atlas and by the Sidi-Saïd-Mâachou volcanosedimentary complex during the Caesaraugustan–middle Languedocian (middle Cambrian) in the Coastal Meseta, marks the northward migration of active rifting structures throughout the Moroccan margin of West Gondwana.

Acknowledgements

The authors are grateful to the reviewers Anne Nédelec and Jean-Paul Liégeois and to the editor-in-chief M. Santosh for their suggestions, which led to great improvement of the original manuscript. This work has been financed by CGL 2006-13533/BTE project, from the Spanish Ministerio de Educación y Ciencia and FEDER, and Portuguese–Moroccan project (GRICES/CNRST). The paper is a contribution to IGCP project 485 ‘Cratons, metacratons and mobile belts: keys from the West African craton boundaries’, and French ANR and ECLIPSE projects.

References

- Ait Ayad, N., Ribeiro, M.L., Mata, J., Ferreira, P., Ezzouhairi, H., Charif, A., Dias, R., 1998. Evolution du magmatisme cambrien en deux régions périgondwaniennes: Azegour (Haut-Atlas) et Alter do Chao-Elvas (NE Alentejo). *Comunicações do Instituto Geológico e Mineiro do Portugal* 84, B154–B157.
- Al-Assam, I., Taylor, B.E., South, B., 1990. Stable isotope analysis of multiple carbonate samples using selective acid extraction. *Chemical Geology* 80, 119–125.
- Albarède, F., 1992. How deep do common basaltic magmas form and differentiate? *Journal of Geophysical Research* 97, 10997–11009.
- Allen, J.R., Matthews, R.K., 1982. Isotopic signature associated with early meteoric diagenesis. *Sedimentology* 29, 791–817.
- Álvaro, J.J., Clausen, S., 2005. Major geodynamic and sedimentary constraints on the chronostratigraphic correlation of the Lower–Middle Cambrian transition in the western Mediterranean region. *Geosciences Journal* 9, 145–160.
- Álvaro, J.J., Clausen, S., 2006. Microbial crusts as indicators of stratigraphic diastems in the Cambrian *Micmacca* Breccia, Moroccan Atlas. *Sedimentary Geology* 185, 255–265.
- Álvaro, J.J., Clausen, S., 2007. Botoman (Lower Cambrian) turbid- and clear-water reefs and associated environments from the High Atlas, Morocco. In: Álvaro, J.J., Aretz, M., Boulvain, F., Munnecke, A., Vachard, D., Vennin, E. (Eds.), *Palaeozoic Reefs and Bioaccumulations: Climatic and Evolutionary Controls*, vol. 275. Geological Society, London, pp. 51–70. Special Publication.
- Álvaro, J.J., Clausen, S., in press. Palaeoenvironmental significance of hatal shell accumulations in a Cambrian intra-cratonic aborted rift, Atlas Mountains, Morocco. *Special Paper on Epeiric Seas*. Geological Association of Canada.
- Álvaro, J.J., Vizcaíno, D., 1997. Episodic development of Cambrian eocrinoid-sponge meadows in the Iberian Chains (NE Spain). *Facies* 37, 49–64.
- Álvaro, J.J., Vizcaíno, D., 1998. Révision biostratigraphique du Cambrien moyen du versant méridional de la Montagne Noire (Languedoc, France). *Bulletin de la Société géologique de France* 169, 233–242.
- Álvaro, J.J., Vizcaíno, D., 2003. The conocoryphid biofacies, a benthic assemblage of normal-eyed and blind trilobites. *Special Papers in Palaeontology* 70, 127–140.
- Álvaro, J.J., Elicki, O., Geyer, G., Rushton, A.W.A., Shergold, J.H., 2003. Palaeogeographical controls on the Cambrian trilobite immigration and evolutionary patterns reported in the western Gondwana margin. *Palaeogeography, Palaeoclimatology, Palaeoecology* 195, 5–35.
- Álvaro, J.J., Ezzouhairi, H., Vennin, E., Ribeiro, M.L., Clausen, S., Charif, A., Ait-Ayad, N., Moreira, M.E., 2006. The Early-Cambrian Boho volcano of the El Graara massif, Morocco: petrology, geodynamic setting and coeval sedimentation. *Journal of African Earth Sciences* 44, 396–410.
- Álvaro, J.J., Ferretti, F., González-Gómez, C., Serpagli, E., Tortello, M.F., Vecoli, M., Vizcaíno, D., 2007. A review of the Late Cambrian (Furongian) palaeogeography in the western Mediterranean region, NW Gondwana. *Earth-Science Reviews* 85, 47–81.
- Álvaro, J.J., Macouin, M., Ezzouhairi, H., Charif, A., Ait-Ayad, N., Ribeiro, M.L., Ader, M., 2008. Late Neoproterozoic carbonate productivity in a rifting context: the Adoudou Formation and its associated bimodal volcanism onlapping the western Saghro inlier, Morocco. In: Ennih, N., Liégeois, J.P. (Eds.), *The Boundaries of the West African Craton*. Special Publication, vol. 297. Geological Society, London, pp. 285–302.
- Badra, L., Pouclet, A., Prost, A.E., Touray, J.C., 1992. Mise en évidence d'une extension intra-plaque tardi-panafricaine d'intérêt métallogénique dans le Haut-Atlas occidental (Maroc). *Comptes Rendus de l'Académie des Sciences* 314, 703–709.
- Bébien, J., 1980. Magmatismes basiques dits “orogéniques” et “anorogéniques” et teneurs en TiO_2 : les associations “isotitanées” et “anisotitanées”. *Journal of Volcanology and Geothermal Research* 8, 337–342.
- Bernardin, C., Cornée, J.J., Corsini, M., Mayol, S., Muller, J., Taychi, M., 1988. Variations d'épaisseur du Cambrien moyen en Meseta marocaine occidentale: signification géodynamique des données de surface et de subsurface. *Canadian Journal of Earth Sciences* 25, 2104–2117.
- Bognadov, Yu.A., Gorshkov, A.L., Bogdanova, O.Yu., Gurvich, E.G., Sivtsov, A.V., 1998. Low-temperature hydrothermal ferromanganese mineral phase in the metalliferous sediments of the TAG field, Mid-Atlantic Ocean. *Oceanology* 38, 107–113.
- Bosence, D.W.J., Bridges, P.H., 1995. A review of the origin and evolution of carbonate mud-mounds. In: Monty, C.L.V., Bosence, D.W.J., Bridges, P.H., Pratt, B.R. (Eds.), *Carbonate Mud-Mounds: Their Origin and Evolution*. Special Publication, vol. 23. International Association of Sedimentologists, pp. 3–9.
- Bouma, A.H., 1960. Sedimentation of some Flysch deposits: a graphic approach to facies interpretation. Elsevier, Amsterdam. 168 pp.
- Bruckschen, P., Oesmann, S., Veizer, J., 1999. Isotope stratigraphy of the European Carboniferous: proxy signals for ocean chemistry, climate and tectonics. *Chemical Geology* 161, 127–163.
- Burgath, K.P., von Stackelberg, U., 1995. Sulfide-impregnated volcanics and ferro-manganese incrustations from the southern Lau Basin (southwest Pacific). *Marine Georesources and Geotechnology* 13, 263–308.
- Cailleux, Y., Deloche, C., Gonord, H., Rolin, P., 1989. Les zones de cisaillement hercynien en basse Meseta marocaine. *Notes et Mémoires du Service Géologique du Maroc* 335, 199–209.

- Chaudhuri, A.K., Saha, D., Deb, G.K., Deb, S.P., Mukherjee, M.K., Ghosh, G., 2002. The Purana Basins of southern Cratonic Province of India — a case for Mesoproterozoic fossil rifts. *Gondwana Research* 5, 23–33.
- Chaudhuri, A.K., Deb, G.K., 2004. Proterozoic rifting in the Pranhita–Godavari valley: implication on India–Antarctica linkage. *Gondwana Research* 7, 301–312.
- Corsini, M., 1988. Relation entre la marge du bassin cambrien et la cinématique hercynienne de la Meseta occidentale du Maroc. PhD, Université Aix-Marseille III, 152 p. (unpubl.).
- Crowley, Q.G., Floyd, P.A., Winchester, J.A., Franke, W., Holland, J.G., 2000. Early Paleozoic rift-related magmatism in Variscan Europe: fragmentation of the Armorican Terrane Assemblage. *Terra Nova* 12, 171–180.
- Daesslé, L.W., Cronan, D.S., Marchig, V., Wiedicke, M., 2000. Hydrothermal sedimentation adjacent to the propagating Valu Fa Ridge, Lau Basin, SW Pacific. *Marine Geology* 162, 479–500.
- Dawson, J.W., 1868. *Acadian Geology, The Geological Structure, Organic Remains and Mineral Resources of Nova Scotia, New Brunswick, and Prince Edward Island*, 2nd ed. Macmillan, London. 694 pp.
- Deckart, K., Bertrand, H., Liégeois, J.P., 2005. Geochemistry and Sr, Nd, Pb isotopic composition of the Central Atlantic Magmatic Province (CAMP) in Guyana and Guinea. *Lithos* 82, 282–314.
- Demicco, R., Hardie, L.A., 1994. Sedimentary structures and early diagenetic features of shallow marine carbonate deposits. *SEPM Atlas Series* 1, 1–265.
- Destombes, J., Jeannette, A., 1966. Mémoire explicatif de la carte géo-technique de la Meseta côtière à l'Est de Casablanca au 1:50 000. Notes et Mémoires du Service Géologique du Maroc 180, 1–104.
- El Attari, A., Hoepffner, C., 1997. Découverte de Brachiopodes à affinité Cambrien supérieur dans le synclinial d'Imfout (Meseta occidentale) et corrélation stratigraphique. 14^{ème} Colloque des B.S.M., Kenitra, 24–27 Septembre, Résumés.
- El Baghdadi, M., El Bouikhari, A., Jouider, A., Benyoucef, A., Nadeem, S., 2001. Petrographic, geochemical and zircon typology of Neoproterozoic granitoids: evidence of continental thickening in Saghro Arc (Eastern Anti-Atlas, Morocco). *Gondwana Research* 4, 612.
- El Baghdadi, M., El Boukhari, A., Jouider, A., Benyoucef, A., Nadeem, S., 2003. Calc-alkaline arc I-type granitoid associated with S-type granite in the Pan-African Belt of Eastern Anti-Atlas (Saghro and Ougnat, South Morocco). *Gondwana Research* 6, 557–572.
- El Hadi, H., Tahiri, A., Simancas Cabrera, F., González Lodeiro, F., Azor Pérez, A., Martínez Poyatos, D.J., 2006. Un exemple de volcanisme calco-alcalin de type orogénique mis en place en contexte de rifting (Cambrien de l'oued Rhebar, Meseta occidentale, Maroc). *Comptes Rendus Géoscience* 338, 229–236.
- El Tabakh, M., Riccione, R., Schreiber, B.C., 1997. Evolution of Late Triassic rift basin evaporites (Passaic Formation): Newark Basin, Eastern North America. *Sedimentology* 44, 767–790.
- Etxebarría, M., Chalot-Prat, F., Apraiz, A., Eguíluz, L., 2006. Birth of a volcanic passive margin in Cambrian time: rift paleogeography of the Ossa-Morena Zone, SW Spain. *Precambrian Research* 147, 366–386.
- Ezzouhairi, H., Ribeiro, M.L., Ait Ayad, N., Moreira, M.E., Charif, A., Ramos, J.M.F., de Oliveira, D.P.S., Coke, C., 2008. The magmatic evolution at the Moroccan outboard of the West African Craton between the Late Neoproterozoic and the Early Palaeozoic. In: Ennih, N., Liégeois, J.P. (Eds.), *The Boundaries of the West African Craton*. Special Publication, vol. 297. Geological Society, London, pp. 329–343.
- Fernández-Mendiola, P.A., García-Mondéjar, J., 2003. Carbonate platform growth influenced by contemporaneous basaltic intrusion (Albian of Larrano, Spain). *Sedimentology* 50, 961–978.
- Flügel, E., 2004. *Microfacies of Carbonate Rocks*. Springer-Verlag, Berlin. 976 pp.
- Furman, T., 1995. Melting of metasomatized subcontinental lithosphere: undersaturated mafic lavas from Rungwe, Tanzania. *Contribution to Mineralogy and Petrology* 122, 97–115.
- Furman, T., 2007. Geochemistry of East African Rift basalts: an overview. *Journal of African Earth Sciences* 48, 147–160.
- Gasquet, D., Levresse, G., Cheilletz, A., Rachid Azizi-Samiz, M., Mouttaqi, A., 2005. Contribution to a geodynamic reconstruction of the Anti-Atlas (Morocco) during Pan-African timers with the emphasis on inversion tectonics and metallogenic activity at the Precambrian–Cambrian transition. *Precambrian Research* 140, 157–182.
- Gerdes, G., Krumbein, W.E., 1994. Peritidal potential stromatolites — a synopsis. In: Bertrand-Sarfati, J., Monty, C. (Eds.), *Phanerozoic Stromatolites II*. Kluwer Academic Publisher, Dordrecht, pp. 101–129.
- Morocco'95. In: Geyer, G., Landing, E. (Eds.), *The Lower-Middle Cambrian standard of Gondwana*. Beringeria, vol. 2, pp. 1–171. Special Issue.
- Gigout, M., 1951. Etudes géologiques sur la Meseta marocaine occidentale (arrière-pays de Casablanca, Mazagan et Safi). Notes et Mémoires du Service Géologique du Maroc 86, 1–507.
- Gigout, M., 1956. Le volcan sous-marin d'âge Acadien de Sidi-Said-Maâchou (Maroc occidental). *Bulletin de la Société géologique de France* 6, 559–574.
- Glasby, G.P., Stuben, D., Jeschke, G., Stoffers, P., Garbe-Schönberg, C.D., 1997. A model for the formation of hydrothermal manganese crusts from the Pitcaim Island hotspot. *Geochimica et Cosmochimica Acta* 61, 4583–4597.
- Goscombe, B.D., Gray, D.R., 2008. Structure and strain variation at mid-crustal levels in a transpressional orogen: a review of Kaoko Belt structure and the character of West Gondwana amalgamation and dispersal. *Gondwana Research* 13, 45–85.
- Gregg, T.K.P., Fink, J., 1995. Quantification of lava flow morphologies through analog experiments. *Geology* 23, 73–76.
- Glumac, B., Walker, K.R., 1998. A Late Cambrian positive carbon-isotope excursion in the southern Appalachians: relation to biostratigraphy, sequence stratigraphy, environments of deposition, and diagenesis. *Journal of Sedimentary Research* 68, 1212–1222.
- Hannington, M.D., Jonasson, I.R., Herzig, P.M., Petersen, S., 1995. Physical and chemical processes of seafloor mineralization at mid-oceanic ridges. In: Humphris, S.E., Zierenberg, R.A., Millaneaux, L.S., Thomson, R.E. (Eds.), *Seafloor Hydrothermal Systems: Physical, Chemical and Geochemical Interaction*. Geophysics Monograph, vol. 91. American Geophysical Union, Washington D.C., pp. 115–157.
- Hillgärtner, H., 1998. Discontinuity surfaces on a shallow-marine carbonate platform (Berriasian–Valanginian, France and Switzerland). *Journal of Sedimentary Research* 68, 1093–1108.
- Hupé, P., 1955. Indices d'une phase tectonique salairière dans l'Anti-Atlas marocain. *Comptes Rendus de l'Académie des Sciences de Paris* 241, 971–973.
- Irvine, A.J., Baragar, W.R.A., 1971. A guide to the chemical classification of the common volcanic rocks. *Canadian Journal of Earth Sciences* 8, 523–548.
- Kampunzu, A.B., Makutu, M.N., Rocci, G., Kramers, J., Pineau, F., Louaradi, I., Tembo, F., 1997. Neoproterozoic alkaline and carbonatite magmatism along the Western rift in Central-Eastern Africa: break-up of Rodinia Supercontinent and reconstruction of Gondwana. *Gondwana Research* 1, 155–156.
- Kampunzu, A.B., Tembo, F., Mattheis, G., Kapenda, D., Huntsman-Mapila, P., 2000. Geochemistry and tectonic setting of mafic igneous units in the Neoproterozoic Katangan Basin, Central Africa: implications for Rodinia break-up. *Gondwana Research* 3, 125–153.
- Kidwell, S.M., 1991. Taphonomic feedback (live/dead interactions) in the genesis of bioclastic beds: key for reconstructing sedimentary dynamics. In: Einsele, G., Ricken, W., Seilacher, A. (Eds.), *Cycles and Events in Stratigraphy*. Springer-Verlag, Berlin, pp. 268–282.
- Kidwell, S.M., Bosence, D.W.J., 1991. Taphonomy and time-averaging of marine shelly faunas. In: Allison, P.A., Briggs, D.E.G. (Eds.), *Taphonomy: Releasing the Data Locked in the Fossil Record*. Topics in Geobiology. Plenum Press, New York, pp. 115–209.
- Kilburn, R.J., 2000. Lava flows and flow fields. In: Sigurdsson, H., Houghton, B., McNutt, S.R., Rymer, H., Stix, J. (Eds.), *Encyclopedia of Volcanoes*. Academic Press, London, pp. 291–306.
- Koch, P.L., Zachos, J.C., Gingerich, P.D., 1992. Correlation between isotope records in marine and continental carbon reservoirs near the Palaeocene/Eocene boundary. *Nature* 358, 319–322.
- Korme, T., Acocella, V., Abebe, B., 2004. The role of pre-existing structures in the origin, propagation and architecture of faults in the Main Ethiopian Rift. *Gondwana Research* 7, 467–479.
- Laamrani El Idrissi, A., 1995. Relation déformations-déplacements le long de failles hercyniennes: système de Bouznika du Cherrat-Ben Slimane et du

- Cherrat-Yquem (Meseta marocaine nord–occidentale). *Bulletin de l'Institut des Sciences de Rabat* 19, 1–16.
- Le Maitre, R.W., Bateman, P., Dudek, A., Keller, J., Lameyre-Le Bas, M.J., Sabine, P.A., Schmid, R., Soerensen, H., Streckeisen, A., Wodley, A.R., Zanettin, B., 1989. A Classification of Igneous Rocks and Glossary of Terms: Recommendations of the International Union of Geological Sciences Subcommission on the Systematics of Igneous Rocks. Blackwell Scientific, Oxford. 193 pp.
- Le Roex, A.P., Spath, A., Zartman, R.E., 2001. Lithospheric thickness beneath the southern Kenya Rift: implication from basalt geochemistry. *Contributions to Mineralogy and Petrology* 142, 89–106.
- Lehman, M.F., Bernasconi, S.M., Barbieri, A., McKenzie, J.A., 2002. Preservation of organic matter and alteration of its carbon and nitrogen isotope composition during simulated and in situ early sedimentary diagenesis. *Geochimica et Cosmochimica Acta* 66, 3573–3584.
- Lüders, V., Pracejus, B., Jalbach, P., 2001. Fluids inclusions and sulphur isotopic studies in probable modern analogue Kuruko-type ores from the Jade hydrothermal field (Central Okinawa Trough, Japan). *Chemical Geology* 173, 45–58.
- Marchig, V., Stackelberg, U., Wiedicke, M., Durn, G., Milovanovic, D., 1999. Hydrothermal activity associated with off-axis volcanism in the Peru Basin. *Marine Geology* 159, 179–203.
- Marshall, J.D., 1992. Climatic and oceanographic isotope signals from the carbonate rock record and their preservation. *Geological Magazine* 129, 143–160.
- Martin, U., Reischmann, Th., Bahlburg, H., Schätz, M., Tait, J., Bachtadse, V., 2003. The Early Palaeozoic break-up of Northern Gondwana: sedimentology, physical volcanology and geochemistry of a submarine volcanic complex in the Bavarian Facies Association, Saxothuringian Basin, Germany. *Gondwana Research* 6, 839–858.
- Mazzini, A., Ivanov, M.K., Parnell, J., Stadnitskaia, A., Cronin, B.T., Poludetskina, E., Mazurenko, L., van Weering, T.C.E., 2004. Methane-related authigenic carbonates from the Black Sea: geochemical characterisation and relation to seeping fluids. *Marine Geology* 212, 153–181.
- Meert, J.G., Lieberman, B.S., 2008. The Neoproterozoic assembly of Gondwana and its relationship to the Ediacaran–Cambrian radiation. *Gondwana Research*. doi:10.1016/j.gr.2007.06.007.
- Mergl, M., 1988. Inarticulate brachiopods of early Middle Cambrian age from the High Atlas, Morocco. *Věstník ústředního ústavu geologického* 63, 291–295.
- Mergl, M., Kordule, V., 2008. New Middle Cambrian lingulate brachiopods from the Skryje-Týovice area (Central Bohemia, Czech Republic). *Bulletin of Geosciences* 83, 11–22.
- Michard, A., 1976. Eléments de Géologie Marocaine. Notes et Mémoires du Service Géologique du Maroc 252, 1–382.
- Mills, R.A., Wells, D., Roberts, S., 2001. Genesis of ferromanganese crusts from the TAG hydrothermal field. *Chemical Geology* 176, 3–293.
- Morad, S.M., Marfil, R., de la Peña, J.A., 1989. Diagenetic K-feldspar pseudomorphs in the Triassic Buntsandstein of the Iberian Range, Spain. *Sedimentology* 36, 635–650.
- Ouali, H., Briand, B., Bouchardon, J.L., El Maâtaoui, M., 2000. Mise en évidence d'un volcanisme alcalin intraplaque d'âge Acadien dans la Meseta nord–occidentale (Maroc). *Comptes Rendus de l'Académie des Sciences* 330, 611–616.
- Ouali, H., Briand, B., El Maâtaoui, M., Bouchardon, J.L., 2001. Les amphibolites de la boutonnière paléozoïque de Midelt (Haute Moulouya, Maroc): témoins d'une extension intraplaque au Cambro–ordovicien. Notes et Mémoires du Service Géologique du Maroc 408, 177–181.
- Ouali, H., Briand, B., Bouchardon, J.L., Capiez, P., 2003. Le volcanisme cambrien du Maroc central: implications géodynamiques. *Comptes Rendus Géosciences* 335, 425–433.
- Pichler, T., Veizer, J., 1999. Precipitation of Fe(III) oxyhydroxide deposits from shallow-water hydrothermal fluids in Tutum Bay, Ambitle Island, Papua New Guinea. *Chemical Geology* 162, 15–31.
- Piqué, A., 1979. Evolution structurale d'un segment de la chaîne hercynienne: la Meseta marocaine nord–occidentale. *Sciences Géologiques, Mémoires Strasbourg* 56, 1–243.
- Piqué, A., 2003. Evidence for an important extensional event during the latest Proterozoic and earliest Paleozoic in Morocco. *Comptes Rendus Géoscience* 335, 865–868.
- Piqué, A., Michard, A., 1989. Moroccan Hercynides: a synopsis. The Paleozoic sedimentation and tectonic evolution at the northern margin of West Africa. *American Journal of Science* 289, 286–330.
- Piqué, A., Bouabdelli, M., Darboux, J.R., 1995. Le rift du Maroc occidental. *Comptes Rendus de l'Académie des Sciences (Série IIa)* 320, 1017–1024.
- Riding, R., 1999. The term stromatolite: towards an essential definition. *Lethaia* 32, 321–330.
- Roussel, J., Bernardin, C., 1991. Structure profonde de la Meseta marocaine d'après les données gravimétriques et sismiques. *Géologie Méditerranéenne* 17, 99–108.
- Schrag, D.P., DePaolo, D.J., Richter, F.M., 1995. Reconstructing past sea surface temperatures: correcting for diagenesis of bulk marine carbonate. *Geochimica et Cosmochimica Acta* 59, 2265–2278.
- Schumacher, D., 1996. Hydrocarbon-induced alteration of soils and sediments. In: Schumacher, D., Abrams, M.A. (Eds.), *Hydrocarbon Migration and its Near-Surface Expression*. American Association of Petroleum Geologists Memoir, vol. 66, pp. 71–89.
- Soulaïmani, A., Bouabdelli, M., Piqué, A.L., 2003. L'extension continentale au Néo-protérozoïque supérieur–Cambrien inférieur dans l'Anti-Atlas (Maroc). *Bulletin de la Société géologique de France* 174, 83–92.
- Stern, R.J., 2008. Neoproterozoic crustal growth: the solid Earth system during a critical episode of Earth history. *Gondwana Research*. doi:10.1016/j.gr.2007.06.006.
- Streng, M., 1999. Early Middle Cambrian representatives of the superfamily Acrotretidea (Brachiopoda) from Morocco. *Zeitschrift der Deutschen Geologischen Gesellschaft* 150, 27–87.
- Sun, S.S., McDonough, W.F., 1989. Chemical and isotopic systematics of oceanic basalts: implications for mantle composition and processes. In: Saunders, A.D., Norry, M.J. (Eds.), *Magmatism in the Oceanic Basins*. Special Publications, vol. 42. Geological Society, London, pp. 313–345.
- Thoral, M., 1946. Conocoryphidae languedociens. *Annales de l'Université de Lyon, Sciences Naturelles (Série 3)* 4, 5–92.
- Van Dover, C.L., 2000. *The Ecology of Deep-Sea Hydrothermal Vents*. Princeton University Press, Princeton. 424 pp.
- Van Valen, R.T., Van der Beek, P.A., Cloetingh, S.A.P.L., 1995. The effect of rift shoulder erosion and stratal patterns at passive margins: implications for sequence stratigraphy. *Earth and Planetary Science Letters* 134, 527–544.
- Vaughan, A.P.M., Pankhurst, R.J., 2008. Tectonic overview of the West Gondwana margin. *Gondwana Research* 13, 150–162.
- Veizer, J., Fritz, P., Jones, B., 1996. Geochemistry of brachiopods: oxygen and carbon isotopic records of Paleozoic oceans. *Geochimica et Cosmochimica Acta* 50, 1679–1696.
- Veizer, J., Ala, D., Azmy, P., Bruckschen, P., Buhl, D., Brhun, F., Carden, G.A.F., Diener, A., Ebneth, S., Godderis, Y., Jasper, T., Korte, C., Pawellek, F., Podlaha, O., Strauss, H., 1999. $^{87}\text{Sr}/^{86}\text{Sr}$, $\delta^{13}\text{C}$, and $\delta^{18}\text{O}$ evolution of Phanerozoic seawater. *Chemical Geology* 161, 59–88.
- Wadleigh, M.M., Veizer, J., 1992. $^{18}\text{O}/^{16}\text{O}$ and $^{13}\text{C}/^{12}\text{C}$ in lower Paleozoic brachiopods: implications for the isotopic composition of sea water. *Geochimica et Cosmochimica Acta* 56, 431–443.
- Wallace, M.W., 1987. The role of internal erosion and sedimentation in the formation of stromatactis mudstone and associated lithologies. *Journal of Sedimentary Petrology* 57, 695–700.
- Wallace, P., Anderson Jr., A.T., 2000. Volatiles in magmas. In: Sigurdsson, H., Houghton, B., McNutt, S.R., Rymer, H., Stix, J. (Eds.), *Encyclopedia of Volcanoes*. Academic Press, London, pp. 149–170.
- Walcott, C.D., 1908. Cambrian Brachiopoda: descriptions of new genera and species. *Smithsonian Miscellaneous Collection* 53, 53–137.
- Walter, L.M., Ku, T.C.W., Muchenbachs, K., Patterson, W.P., Bonnell, L., 2007. Controls on the $\delta^{13}\text{C}$ of dissolved inorganic carbon in marine pore waters: an integrated case study of isotope exchange during syndepositional recrystallization of biogenic carbonate sediments (South Florida Platform, USA). *Deep-Sea Research II* 54, 1163–1200.
- Wilson, M.E.J., 2000. Tectonic and volcanic influences on the development and diachronous termination of a Tertiary tropical carbonate platform. *Journal of Sedimentary Research* 70, 310–324.
- Wilson, M.E.J., Lockier, S.W., 2002. Siliciclastic and volcanoclastic influences on equatorial carbonates: insights from the Neogene of Indonesia. *Sedimentology* 49, 583–601.